

Rapid Evolution of the Innermost Dust Disk of Protoplanetary Disks Surrounding Intermediate-mass Stars

Chikako Yasui,^{1*} Naoto Kobayashi,² Alan T. Tokunaga³ and Masao Saito⁴

¹*Department of Astronomy, Graduate School of Science, University of Tokyo, Hongo 7-3-1, Bunkyo-ku, 113-0033, Tokyo, Japan*

²*Institute of Astronomy, School of Science, University of Tokyo, 2-21-1 Osawa, Mitaka, Tokyo 181-0015, Japan*

³*Institute for Astronomy, University of Hawaii, 2680 Woodlawn Drive, Honolulu, HI 96822, USA*

⁴*National Astronomical Observatory of Japan 2-21-1 Osawa, Mitaka, Tokyo, 181-8588, Japan*

23 May 2014

ABSTRACT

We derived the intermediate-mass ($\simeq 1.5\text{--}7\,M_{\odot}$) disk fraction (IMDF) in the near-infrared *JHK* photometric bands as well as in the mid-infrared (MIR) bands for young clusters in the age range of 0 to ~ 10 Myr. From the *JHK* IMDF, the lifetime of the innermost dust disk (~ 0.3 AU; hereafter the *K* disk) is estimated to be ~ 3 Myr, suggesting a stellar mass (M_*) dependence of *K*-disk lifetime $\propto M_*^{-0.7}$. However, from the MIR IMDF, the lifetime of the inner disk (~ 5 AU; hereafter the MIR disk) is estimated to be ~ 6.5 Myr, suggesting a very weak stellar mass dependence ($\propto M_*^{-0.2}$). The much shorter *K*-disk lifetime compared to the MIR-disk lifetime for intermediate-mass (IM) stars suggests that IM stars with *transition disks*, which have only MIR excess emission but no *K*-band excess emission, are more common than classical Herbig Ae/Be stars, which exhibit both. We suggest that this prominent early disappearance of the *K* disk for IM stars is due to dust settling/growth in the protoplanetary disk, and it could be one of the major reasons for the paucity of close-in planets around IM stars.

Key words: circumstellar matter – planetary systems: formation – planetary systems: proto-planetary discs – stars: pre-main-sequence – infrared: stars – stars: variables: T Tauri, Herbig Ae/Be.

1 INTRODUCTION

Understanding protoplanetary disks is not only essential for understanding the star formation process, it is also critical for understanding planet formation (e.g. Lada & Lada 2003). The lifetime of protoplanetary disks is one of the most fundamental parameters of a protoplanetary disk because it directly restricts the time for planet formation (e.g. Williams & Cieza 2011). Many studies that derive the lifetime of protoplanetary disks are now available. In a pioneering work, Strom et al. (1989) studied the frequency of disk-harboring stars with known ages in the Taurus molecular cloud that have a *K*-band excess and suggested that the disk lifetime is in the range from $\ll 3$ Myr to ~ 10 Myr. Subsequently, a more direct method using the ‘disk fraction’, which is the frequency of near-infrared (NIR) or mid-infrared (MIR) excess stars within a young cluster *with an assumed age*, has been widely adopted to study the disk lifetime following the work by Lada (1999) and

Haisch, Lada & Lada (2001a). Using the disk fraction that monotonically decreases as a function of cluster age, the disk lifetime is estimated at about 5–10 Myr in the solar neighborhood (Lada 1999; Haisch et al. 2001a; Hernández et al. 2008; see also Yasui et al. 2010). Mamajek (2009) compiled disk fractions for about 20 clusters and derived the characteristic disk decay time-scale (τ) of 2.5 Myr, assuming the disk fraction[%] $\propto \exp(-t[\text{Myr}]/\tau)$.

These estimated disk lifetimes were mainly derived from the disk fraction with all detected cluster members and thus the estimated lifetime has been primarily for low-mass stars ($< 2\,M_{\odot}$), considering the characteristic mass of the initial mass function (IMF) ($\sim 0.3\,M_{\odot}$, Elmegreen 2009) and the typical stellar mass detection limit ($\sim 0.1\,M_{\odot}$). However, a number of assessments of the effect of the stellar mass dependence of the disk lifetime have recently suggested a shorter disk lifetime for the higher-mass stars (e.g. Hernández et al. 2005; Carpenter et al. 2006; Kennedy & Kenyon 2009). Although the existence of disks of high-mass stars ($\gtrsim 8\,M_{\odot}$) is still under debate (e.g. Mann & Williams 2009; Fuente et al. 2002), the disks of IM stars have been extensively studied

* E-mail: ck.yasui@astron.s.u-tokyo.ac.jp (CY)

and are well characterized (Hernández et al. 2005, 2007a, 2008). IM stars with optically thick disks are known as Herbig Ae/Be (HAeBe) stars. They were originally discovered with strong emission-lines by Herbig (1960). After Hernández et al. (2004) established the method for selecting HAeBe stars using the spectral energy distribution (SED) slope from the *V*-band to the IRAS 12- μ m band, Hernández et al. (2005) derived the HAeBe-star disk fraction for six clusters in the age range of 3–10 Myr. They showed that the disk fraction is lower compared to the previously derived disk fraction for low-mass (LM) stars, in particular by a factor of ~ 10 lower at ~ 3 Myr.

Recently, the disk fraction studies have shifted to longer wavelengths (MIR or submm) mainly because of the interest in tracing the outer disk, where most of the disk mass resides (Williams & Cieza 2011). However, the disk fractions can also be estimated using only *JHK* data, in particular, for the IM stars. Originally, the disk lifetime was estimated with disk fractions derived by using the color-color diagram based on imaging in the *JHK* and *JHKL* photometric bands (e.g. Haisch et al. 2001a; Lada 1999). After the advent of the *Spitzer Space Telescope*, the SED slope ($\alpha = d \ln \lambda F_\lambda / d \ln \lambda$) in the MIR wavelength range (3.6, 4.5, 5.8, and 8.0 μ m) is used for selecting disk-harboring stars (e.g. $\alpha \geq -2.0$; Lada et al. 2006). However, the derived disk fractions and disk lifetime with *Spitzer* data were found to be almost the same as those with *JHKL* data (see Sicilia-Aguilar et al. 2006; Hernández et al. 2008), and even with *JHK* data (Lada 1999; Yasui et al. 2010). Although the NIR disk fractions are known to show values systematically smaller and with a larger uncertainty due to contamination of the non-disk-harboring stars on the colour-colour diagram (Haisch et al. 2001b; Yasui et al. 2010), Hernández et al. (2005) showed that the *JHK* colour-colour diagram can clearly distinguish disk-harboring IM stars from non-disk IM stars. The *JHK* disk fraction value is robust both because of the large infrared excess and the higher stellar effective temperature of the IM stars, compared to LM stars.

In this paper, we derived the *JHK* IMDF using the Two Micron All Sky Survey (2MASS) Point Source Catalog of a large number (~ 20) of well-established nearby ($D \lesssim 1.5$ kpc) young clusters with an age span of 0 to ~ 10 Myr in order to quantitatively and comprehensively study the lifetime of protoplanetary disks surrounding IM stars ($\simeq 1.5\text{--}7 M_\odot$). In particular, we included as many clusters as possible with ages < 5 Myr. To securely identify IM cluster members, we made use of the spectral types of each cluster member from the literature, assuming a single age for each cluster. With the derived *JHK* IMDFs for a large number of younger clusters (< 5 Myr), we estimated the disk lifetime of the IM stars. We then estimated the stellar mass dependence of the disk lifetime by comparing the lifetime of IM stars to that of LM stars. We also derived the MIR IMDFs with *Spitzer* data in the literature to compare them to the *JHK* IMDFs. We found that the derived *JHK* IMDFs are significantly lower than the MIR IMDFs, in particular at younger ages (< 3 Myr), which results in shorter lifetime of the *K* disk than the MIR disk. This suggests a potentially larger fraction of ‘transition disks’ for IM stars compared to those for LM stars. We discuss the implications of these results for dust growth and planet formation.

Because the sample clusters and the selection of the IM stars is critical for this paper, we discuss this in detail in Section 2. The definition and derivation of the *JHK* IMDF and the MIR IMDF are described in Sections 3 and § 4, respectively. Before interpreting the results of the IMDFs, the definition of the disk lifetime is discussed in Section 5. Section 6 then discusses the results for *JHK* IMDFs. The mid-IR disk fraction is discussed in Section 7. Subsequently, Section 8 discusses the large difference between *JHK* and MIR IMDFs found in this study and potential disk evolution consequences for IM stars. Finally, Section 9 discusses the possible physical mechanisms of this rapid evolution of the *K* disk. At the end, in Section 10, we briefly discuss possible implications for planet formation. Section 11 summarizes this paper.

2 TARGET CLUSTERS AND SELECTION OF INTERMEDIATE-MASS STAR SAMPLES

2.1 Target clusters

We selected our target clusters from previous studies of the disk fraction/disk evolution (Haisch et al. 2001a; Hernández et al. 2005, Hernández et al. 2008; Kennedy & Kenyon 2009; Mamajek 2009; Gáspár et al. 2009; Fedele et al. 2010; Roccatagliata et al. 2011). For estimating the disk lifetime with acceptable accuracy, it is necessary to derive the IMDFs for as many as young clusters as possible, ideally more than ten. We thus selected our target young clusters from the above papers, but with the following criteria: (1) Cluster ages are spaced from 0 to ~ 10 Myrs, to cover the time period of disk dispersal. (2) The cluster membership is well defined from a variety of observations (astrometry, radial velocity, variability, $H\alpha$, X-ray, NIR excess, MIR excess, optical spectroscopy, NIR spectroscopy, etc.). This criterion naturally leads to clusters in the solar neighborhood (distance < 1.5 kpc). (3) The spectral types of a large number of cluster members are available by spectroscopy. (4) Well-defined NIR and MIR photometry of the cluster members with $M_{\text{limit}} \sim 1 M_\odot$ is published or in a widely available catalogue, such as 2MASS. (5) At least three IM stars are available per cluster for IMDF derivation.

The resultant 19 target clusters are summarized in Table 1 along with the age, distance, and references for the disk fraction study. Almost all young (< 5 Myr) clusters in the references (Table 1) are included, though three young clusters (MBM 12, NGC 6231, and NGC 7129) are excluded. This is because it appears that no IM stars are present in MBM 12 (Luhman 2001) and the spectral types of stars in NGC 6231 and NGC 7129 are limited only to brightest members (OB, A stars), and is not adequate to cover the entire IM star mass range down to $1.5 M_\odot$. Some older clusters (> 5 Myr), mostly those from Fedele et al. (2010), are excluded because they do not satisfy the above criterion. For several well-known clusters within the target clusters (Trapezium, Ori OB1a, Ori OB1bc, Per OB2), we could derive only *JHK* disk fractions because we could not find published *Spitzer* MIR data for the IM stars, probably because of saturation. As a result, we obtained the *JHK* IMDF for 19 clusters and the MIR IMDF for 13 clusters.

2.2 Selection of intermediate-mass stars

Although the original definition of mass for HAeBe is $\sim 2\text{--}10 M_{\odot}$ with spectral types of B and A (and in a few cases F) (Herbig 1960), the presence of disks around stars earlier than B5 ($\simeq 6\text{--}7 M_{\odot}$ in the main-sequence phase) is not well established since the disk lifetime of high-mass stars is very rapid, e.g. ~ 1 Myr (Zinnecker & Yorke 2007; Fuente et al. 2002). Also, the number of high-mass stars ($> 6\text{--}7 M_{\odot}$) is very small because of the IMF, and the number stochastically fluctuates from cluster to cluster. Therefore, we set the upper-mass limit as $7 M_{\odot}$ in this paper. This is also a good match with the mass range of the isochrone model by Siess, Dufour & Forestini (2000) ($M_{\text{max}} = 7 M_{\odot}$), which is used throughout this paper. As for the lower-mass limit, we employed $1.5 M_{\odot}$, which corresponds to spectral type ‘F1’ for main sequences, following past comprehensive works of disks for IM stars by Hernández et al. (2005) and Kennedy & Kenyon (2009). The latter defined a mass range bin of $1.5\text{--}7 M_{\odot}$, which can be directly compared to our results.

The IM star selection is a critical item for this study. Ideally, stellar mass and the age of each cluster member are determined from the HR diagram with the extinction-corrected luminosity and spectroscopically determined effective temperature through an isochrone model. However, this requires a time-consuming observational program, and thus the number of target clusters is limited as in the previous studies. Even if we had the complete observational data, the value of mass and age depends on the isochrone model, and could strongly depend on the extinction correction with different R_V (e.g. Hernández et al. 2004, 2005). Another approach is to use a limited number of parameters, such as only the spectral type, to pick up cluster members in a broad mass range, such as IM or LM stars, and to use a larger number of clusters. Although sacrificing the accuracy of the mass estimate, a study including a larger number of clusters is possible. Although some past studies, in fact, focus on targets of certain spectral types (e.g. earlier than F1) to pick up IM stars (Hernández et al. 2005; Uzpen, Kobulnicky & Kinemuchi 2009), *the true mass for a star of a certain spectral type varies with the age of the star*, and such spectral-type-limited samples should be viewed with caution (Kennedy & Kenyon 2009). We assume the cluster age is the age of the members in the selection of the IM stars.

The choice of the isochrone model is critical for the mass estimate. Although a number of recent isochrone models are available (e.g., such as Yi, Kim, & Demarque 2003; Tognelli, Prada Moroni, & Degl’Innocenti 2011), we choose Siess et al. (2000) because it is the most used isochrone track in the target mass range with the reliability through various tests and application to many observational data. Using dynamically and kinematically determined stellar masses, Hillenbrand & White (2004) confirmed that virtually any isochrone model provides similar mass estimate for masses more than $1.2 M_{\odot}$. Hillenbrand & White (2004) also noted that the introduction of new isochrone models tend to bring new systematic uncertainty and should be used with caution. For this study, using Siess’s isochrone is also critical for comparison with the previous studies which used Siess’s isochrone in most cases (e.g., Kennedy & Kenyon 2009).

We take particular note of the fact that the age spread of young clusters in the solar neighborhood is in many cases small enough so that a single age can be assumed for each cluster (see Table 1). Therefore, the boundary masses of the IM stars (7 and $1.5 M_{\odot}$) theoretically correspond to a unique spectral type for each cluster, which enables IM star selection only with the spectral type of the members without considering differential extinction. This method should be effective, in particular, for IM stars because most of the time they evolve along the Henyey track, which is roughly horizontal on the HR diagram, and even when the IM stars are on Hayashi track before switching to the Henyey track, the spectral type does not change because the track is almost vertical on the HR diagram. Table 2 shows the unique spectral types corresponding to the boundary masses for each cluster age based on the isochrone model by Siess et al. (2000).

However, there are several points to take note for using the above method in selecting the IM stars. First, each spectral type, in particular the later spectral type (G7–K5), corresponds to a slightly broader mass range as shown in the third column of Table 2. For example, the boundary spectral type K5 corresponds to $1.2\text{--}1.5 M_{\odot}$ for the age of 2 Myr. Therefore, the sampling by spectral type naturally leads to the inclusion of stars with a mass of slightly lower than the nominal $1.5 M_{\odot}$. Next, note that the age spread of each cluster may cause contamination of lower-mass stars in our IM-star samples in the case where the age of the star is older than the cluster age. Table 2 also shows the possible mass range for an age spread of $\Delta t = 2$ Myr, which is the maximum possible age spread in most cases (typically $\Delta t = 1$ Myr: see Table 1). Although the age of most stars are within the age spread of 2 Myr, there are $\sim 15\%$ stars at most which are older than the age spread and are actually lower-mass stars (see Figs. 1–5 in Palla & Stahler 2000). Lastly, the distance uncertainties of target clusters may also influence on the selection of the IM stars. The typical uncertainties of distance is about 10% for the clusters in the solar neighborhood (Reipurth 2008a,b). For the clusters studied by Hernández et al. (2005), the uncertainties are even smaller (less than 5%) with *Hipparcos* data. For deriving the mass and age of a star on H-R diagram, the effective temperature is independent of the distance because it is derived from spectroscopy, while luminosity is directly affected. However, the luminosity can differ by only 0.2 mag with the assumed distance uncertainties, which then cause a mass difference of $\lesssim 0.1 M_{\odot}$ around lower mass limit of this study, $1.5 M_{\odot}$ ¹, from the isochrone models by Siess et al. (2000) in the target age range of this paper (≤ 11 Myr). Because this mass uncertainty is very small, the distance uncertainties for the selection of IM stars does not affect our results. The above three points (or any other unconsidered uncertainties) might mask the possible lifetime difference between IM and LM stars. However, if we find any significant difference, it is likely to be real and should be clearly seen with better selected IM-star samples in the future. Note that contamination of higher-mass stars can occur, but that

¹ Note that the age differences are ≤ 1 Myr for stars ≤ 3 Myr and $\lesssim 2$ Myr for older stars. These differences are within the age spread (2 Myr) we are considering.

should not affect the lifetime differences between the disks of IM and LM stars. We discuss the effect of IM star selection on the derived IMDF in section 8.1.2.

2.3 Selected samples

We searched the literature to gather all of the available spectral type information for the stars in the sample clusters. We then made a list of all the IM stars by selecting cluster members by spectral type earlier than that of the lower-mass boundary and also later than that of the higher-mass boundary. The clusters chosen are shown in column 1 and the references to the papers from which the IM stars were selected is shown in column 2 of Table 3. Following the fifth criterion in Section 2.1, we removed any target clusters for which less than three IM stars can be identified. Also, because IMDFs for clusters with age of >5 Myr are found to be $\simeq 0$ per cent as discussed in the following sections, we obtained IMDFs for only about 10 clusters. Disk fractions for clusters with age of ≤ 5 Myr are the most useful for studying stellar mass dependence of disk dispersal (cf. Kennedy & Kenyon 2009).

As a result, the total number of stars used for deriving *JHK* and *MIR* IMDF become 799 and 365, respectively. In Appendix A, the IM star samples for all clusters are summarized in tables as well as in colour-colour diagrams. For the following five clusters, the spectral type information for lower-mass stars in the literatures is incomplete, and we could not reach to the mass-limit of $1.5 M_{\odot}$: γ Vel (F5: $2 M_{\odot}$), λ Ori (G0: $2 M_{\odot}$), Per OB2 (G8: $1.8 M_{\odot}$), OB1bc (G3: $2.2 M_{\odot}$), and OB1a (G6: $1.7 M_{\odot}$). Although it is desirable to set exactly the same mass limit, such as $2 M_{\odot}$, we used $1.5 M_{\odot}$ as the lowest mass for the other clusters in order to obtain as many IM stars as possible.²

3 *JHK* IMDF

The optical-NIR SED difference between stars with and without disks is more prominent for IM stars than LM stars (Lada & Adams 1992; Carpenter et al. 2006). This is mainly because the stellar SED for stars with higher masses peaks at the shorter wavelength side of the *U* and *B* bands (e.g. $\sim 0.3 \mu\text{m}$ for A0V stars, with mass of $\sim 3 M_{\odot}$ and T_{eff} of 9790 K; Cox 2000) compared to the disk SED that peaks near the *K* band ($\gtrsim 2 \mu\text{m}$). HAeBe stars also have a large infrared excess from the optically thick disk ‘wall’, which arises from the inner edge of the disks and where dust disk is so hot as to evaporate (Natta et al. 2001; Dullemond, Dominik & Natta 2001). Therefore, even in the case of using only *JHK* photometry, IM stars with disks can be much more easily and more accurately selected than LM stars with disks. Indeed, Hernández et al. (2005) found an intrinsic region for HAeBe stars on a *JHK* colour-colour diagram (see their fig. 2). Also, the photometric uncertainties for IM stars in nearby clusters are very small, typically $\lesssim 0.02$ mag for all *JHK*-bands. We make use of these characteristics to derive the *JHK* IMDF for each target cluster with the selected sample of IM stars.

² We checked how much the IMDF changes with a mass limit of $2 M_{\odot}$ and confirmed that the resultant IMDFs do not change within the uncertainty.

3.1 Identification of IM stars in the colour-colour diagram

On the *JHK* colour-colour diagram, the stars with disks are known to be lying in the infrared-excess region that is separated from the region of stars without disks (e.g. Lada & Adams 1992). For low-mass stars, disk fractions of various young clusters have been derived using *JHK* colour-colour diagram (Lada 1999; Yasui et al. 2010; see also Hillenbrand 2005). For IM stars, Lada & Adams (1992) showed that HAeBe stars occupy completely separated regions even from those for classical Be (CBe) stars based on the modelling of disk emission. CBe stars show near-infrared excess from gaseous free-free emission and are often confused with HAeBe stars, but the disk excess from HAeBe stars is much larger. After Hernández et al. (2005) defined the locus of HAeBe stars on the intrinsic *JHK* colour-colour diagram, Wolff, Strom & Rebull (2011) identified HAeBe stars of IC 1805 using their definition. Comerón et al. (2008a) defined the disk excess region for HAeBe stars on the *JHK* colour-colour diagram (non-intrinsic) by using a line that passes through $(H - K, J - H) = (0.11, 0)$ and is parallel to the reddening vector as a border-line between the HAeBe stars and CBe stars.

In Fig. 1, we plot the *observed* colors of the HAeBe stars (filled circles) and the CBe stars (open circles) for all the samples in Hernández et al. (2005, Upper Sco, Lac OB1, Ori OB 1a, Ori OB 1bc, and Tr 37) on the *JHK* colour-colour diagram. This shows that the HAeBe stars are spatially separated from the main-sequence track (Bessell & Brett 1988, black line in the colour-colour diagram). Note that the data points shown are not corrected for reddening. There is a clear division between HAeBe stars and other objects, and a border-line can be set as the dot-dashed line, which passes through the point of $(H - K_S, J - H) = (0.2, 0)$ and is parallel to reddening vector (black arrow). This border-line is slightly shifted to the right compared to Comerón et al.’s border-line (Fig. 1) to completely avoid contamination from CBe stars. Hereafter, we call the right-side region of the border-line the ‘IM disk excess region’ (orange shaded region). This border-line is more precise for dividing HAeBe stars and CBe stars than that of Comerón et al. (2008a) (gray dot-dashed line in Fig. 1) because some CBe stars are included in the IM disk excess region when using Comerón’s border-line. Therefore, we use the line passing through $(H - K_S, J - H) = (0.2, 0)$ as the border-line, and the *JHK* IMDF is defined to be the ratio of the stars located in the IM disk excess region to the total number of stars in a cluster that are selected with the criteria in Section 2.2.

Note that there is a well-known classification for HAeBe stars by Meeus et al. (2001), Group I for younger flared disk phase and Group II for older flat disk phase. We confirmed that all stars in Group I and II, except for one star (HD 135344 in Group I) out of 14 stars, are recognized as HAeBe stars in our method.

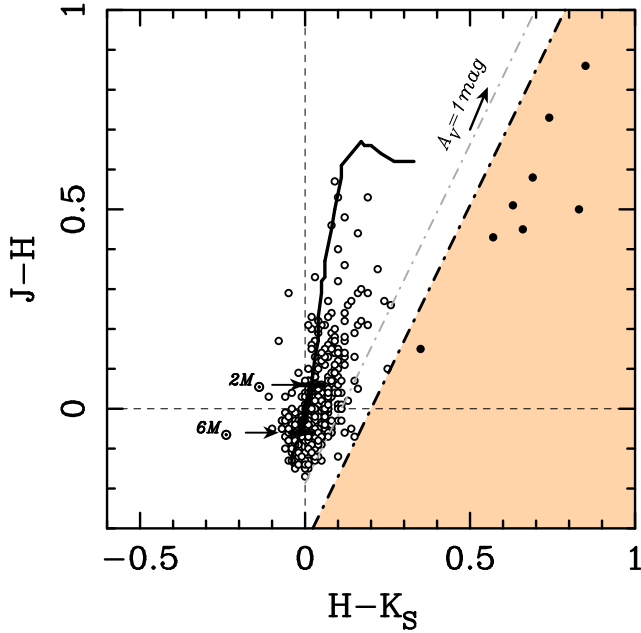


Figure 1. *JHK* colour-colour diagram for IM stars. The observed colours of H AeBe stars (filled circles) and C Be stars (open circles) in nearby clusters from Hernández et al. (2005, Upper Scorpius, Per OB2, Lac OB1, Ori OB1a, and Ori OB1bc) are shown with the dwarf track (Bessell & Brett 1988) (black line). The estimated border-line, which is parallel to the reddening vector and distinguishes H AeBe stars from other objects, is shown with a dot-dashed line: the gray dot-dashed line shows the definition by Comerón et al. (2008a) while the black dot-dashed line shows our definition. The region to the right of the border-line (orange color) is defined as the ‘IM disk excess region’.

3.2 Determination of the IMDF

We used the 2MASS Point Source Catalog³ to obtain the *JHK* magnitudes of all the sample IM stars. We rejected all IM stars that do not have an ‘A’ photometric quality flag (signal-to-noise ≥ 10 for all *JHK* bands) in the 2MASS catalogue. We then obtained the IMDF of the IM stars from the *JHK* colour-colour diagrams of each target cluster.

From previous studies of the disk fractions for low-mass stars, the systematic errors of the disk fraction are known to be less than the statistical errors when using data with small photometric uncertainties (Liu, Najita & Tokunaga 2003; Yasui et al. 2009). The present data should be in the same situation in view of the small uncertainties in *JHK* photometry of the IM star samples. For estimating the statistical errors of the disk fraction, we assumed that the errors are dominated by Poisson errors ($\sqrt{N_{\text{disk}}}$), and we used $\sqrt{N_{\text{disk}}}/N_{\text{all}}$ for the one-sigma uncertainty of the disk fraction, where N_{disk} is the number of stars with optically thick disks (= H AeBe stars) and N_{all} is the number of all cluster members, respectively. However, if the number of H AeBe stars is zero, the statistical error was calculated assuming one H AeBe star in the examined target cluster to give a one-sigma uncertainty of $1/N_{\text{all}}$ (e.g. Hernández et al. 2005).

Table 3 summarizes the derived *JHK* IMDFs for all the target clusters.

4 MIR IMDF

In the previous studies utilizing the data from the *Spitzer Space Telescope*, the SED slope ($\alpha = d \ln \lambda F_{\lambda} / d \ln \lambda$; Adams, Lada & Shu 1987) in the MIR wavelength range (3.6, 4.5, 5.8, and 8.0 μm) is used for selecting disk-harboursing stars (e.g. $\alpha \geq -2.0$; Lada et al. 2006; Hernández et al. 2007b). The number of such IM stars should be precisely determined with this method since disks show a large flux excess compared to the central star continuum in the MIR. For the derivation of the MIR IMDF, we made use of the published *Spitzer* photometric results in the literature because of the signal-to-noise and uniformity across target clusters.

For the definition of the MIR disk fraction, we followed the procedure by Kennedy & Kenyon (2009), who derived α using the SED slope of *Spitzer*’s Infrared Array Camera (IRAC) [3.6] to [8] and regarded those with $\alpha > -2.2$ as cluster members with MIR dust disks. We estimated α of the IM stars only in the cases where reliable photometry in all four IRAC bands is available. However, for the derivation of α , we used only [3.6] and [8.0] because those two bands determine α for almost all cases. For several clusters (e.g. IC 348, which shows moderate extinction), we cross-checked our α values with those in the literature (Hernández et al. 2008) and confirmed that they are almost the same. Following Kennedy & Kenyon (2009), we set the boundary at $\alpha = -2.2$ to separate all the IM stars into the categories of ‘with disk’ and ‘without disk’.

For the target clusters with published *Spitzer* data (13 clusters out of 19 target clusters; see Table 3), we estimated α for the IM stars. Unfortunately, the MIR *Spitzer* photometry of some IM stars in the nearby star-forming regions could not be obtained because they are too bright for *Spitzer*. Therefore, the number of IM stars for the MIR IMDF is, in most cases, less than those for the *JHK* IMDF (e.g. Tr 37). In some cases, we have more sample stars for the MIR than those for *JHK* (e.g. λ Ori) because some of the MIR stars do not have good *JHK* photometry with 2MASS. In this case, we calculated the MIR IMDF by rationing the number of stars with disks by the total number of stars in each MIR sample. The results are summarized in Table 3. The treatment of uncertainty is similar to that for the *JHK* IMDF, as described in Section 3).

5 DEFINITION OF THE DISK LIFETIME

Different terms have been used for the disk dispersal time-scale; e.g. disk lifetime (Lada 1999; Haisch et al. 2001a; Hernández et al. 2008), disk decay time-scale (Mamajek 2009), and disk dissipation time-scale (Fedele et al. 2010). These terms are based on the observed cluster age-disk fraction plot with age on the horizontal axis and disk fractions on the vertical axis. However, these terms are not consistently used. Moreover, the value of disk fraction at zero age has not been considered with care because these studies are performed mainly for low-mass stars and all low-mass stars

³ http://www.ipac.caltech.edu/2mass/releases/allsky/doc/sec6_2ptinfo.html

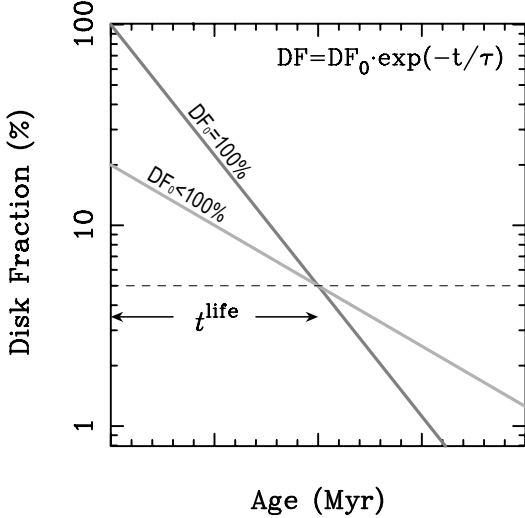


Figure 2. Definitions of disk decay time-scale (τ), disk lifetime (t^{life}), and initial disk fraction (DF_0).

are thought to initially have disks in the standard picture of low-mass star formation (Shu, Adams & Lizano 1987). Since this may not be the case for IM stars, we define these terms explicitly in this section.

To fit with a single function to the disk fraction evolution curve, an exponential function is appropriate. The ‘disk decay time-scale’ (τ) is defined as: $DF[\%] \propto \exp(-t[\text{Myr}]/\tau)$ (e.g. Mamajek 2009). The decay time-scale is proportional to the slope of the curve on a semilog plot, $\log(\text{IMDF})$ –age plot (Fig. 2). On the other hand, the most often used term ‘disk lifetime’ (t^{life}) is originally defined as the x -intercept of the cluster age–disk fraction plotted as a linear function. However, fitting with a linear function does not appear appropriate to describe the shape of disk fraction evolution, which appears to decrease and level out at about 5–10 per cent (Hernández et al. 2008). Therefore, we define the disk lifetime to be the time when the disk fraction is 5 per cent (t^{life}) and use this for the discussion throughout this paper.

We define the ‘initial disk fraction’ (DF_0) as the disk fraction at $t = 0$. Fig. 2 shows two possible cases: $DF_0 = 100$ per cent and $DF_0 < 100$ per cent for the same t^{life} . The value of $DF_0 = 100$ per cent (the dark gray line in Fig. 2) means that all stars initially have disks, while that of $DF_0 < 100$ per cent (the light gray line in Fig. 2) means that all stars do not necessarily have disks from the beginning or that some disks disappear quickly within a very short time-scale that is not recognized within the accuracy of the age determination. Note that if DF_0 is constant, then the disk lifetime is proportional to disk decay time-scale.

6 EVOLUTION OF THE K DISK

The stellocentric distance of the K disk (r_K) for H AeBe stars has a wide range, ~ 0.1 – 1.0 AU for H Ae stars to ~ 1 – 10 AU for H Be stars (Millan-Gabet et al. 2007). However, because a large part of the IM stars in this paper are H Ae stars, r_K of ~ 0.3 AU is taken to be the nominal radius in this paper. The JHK IMDF derived in this paper is the fraction of the H AeBe stars whose disks at a stellocentric distance

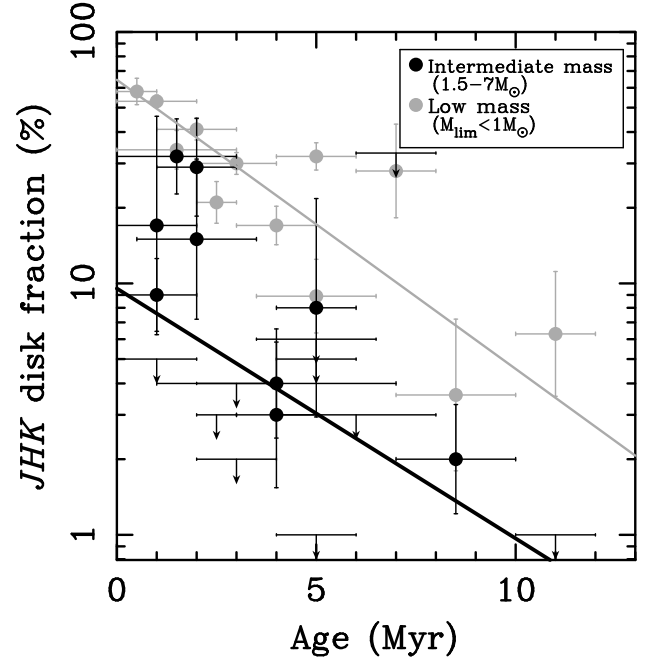


Figure 3. JHK IMDF (black) and JHK LMDF (gray) of young clusters in the solar neighbourhood as a function of cluster age. For the IMDF, the data for clusters in Table 3 are shown with black filled circles, while upper-limits are shown with downward arrows. The fitted curve with the survival analysis for all the clusters, including the upper limits is shown with the black line. For comparison, the LMDF from Yasui et al. (2009, 2010) is shown with the gray line.

(r_K) of ~ 0.3 AU are optically thick with a temperature of ~ 1500 K (see e.g. fig. 2 in Millan-Gabet et al. 2007).

In this section, we discuss the evolution of the K disk of IM stars traced by K band excess emission and on the JHK IMDF change with cluster age.

6.1 Disk lifetime

By making use of the method described in Section 3, the JHK IMDFs of ~ 20 clusters are derived for the first time, in particular for clusters at ages < 3 Myr. Fig. 3 shows the derived IMDF as a function of ages (black filled circles). The JHK IMDF is found to show an exponentially decreasing trend with increasing cluster age as seen in previous studies. There is a large scatter with many upper-limits at 1–3 Myr. In view of the upper-limit points, we used the astronomical survival analysis methods (Isobe et al. 1986; Lavalley, Isobe & Feigelson 1992) as a primary analysis tool. We used the `schmidttdbin` task in the `iraf/stsdas` package. The resultant disk decay time-scale is $\tau = 4.4 \pm 2.2$ Myr with $DF_0 = 10 \pm 4$ per cent. The resulting disk lifetime is $t_{\text{IM},JHK}^{\text{life}} = 2.8 \pm 2.4$ Myr. The fitted curve is shown in Fig. 3 as a thick black line. We refer to this fitting as ‘survival fitting’.

The IMDF data points at ages < 3 Myr show a rather large scatter with upper-limit points. The clusters with zero disk fraction (ρ Oph, IC 348, σ Ori, NGC 2264) do not appear to have obvious common features. As for the initial disk fraction (DF_0), the fitting results show a low value

of <20 per cent. Although some non-zero data points at 1–2 Myr are apparently above the fitted line, all of them show relatively low values that are not more than ~ 40 per cent. Whether all high-mass stars initially have disks or not is still under debate (e.g. Zinnecker & Yorke 2007). On the other hand, all low-mass stars, are thought to initially have disks in the standard picture of low-mass star formation (Shu et al. 1987). Our results suggest a possible low initial disk fraction for IM stars, and further study of the IMDF is important, in particular, those of the younger clusters.

6.2 Comparison with low-mass stars

In Fig. 3, we show the *JHK* LMDF for comparison. The LMDF data points are for 12 clusters in the solar neighbourhood from Yasui et al. (2009, 2010). The fitting result of LMDFs is shown with a gray line (Fig. 3), which has $\tau_{\text{LM},JHK} = 3.8 \pm 0.4$ Myr and $\text{LMDF}_{0,JHK} = 64 \pm 6$ per cent, leading to a disk lifetime of $t_{\text{LM},JHK}^{\text{life}} = 9.7 \pm 1.1$ Myr. Fig. 3 clearly shows the difference in the disk fraction value, as well as the disk lifetime difference, between the IM and LM stars. The IMDFs for older clusters (age > 3 Myr) show systematically lower values compared to the LMDF, as Hernández et al. (2005) initially found for 5 clusters (Tr 37, Ori OB1bc, Upper Sco, Per OB2, and Ori OB1a). We increased the number of target clusters of age >3 Myr to 10 and confirmed this tendency. However, while fig. 10 in Hernández et al. (2005) shows an IMDF curve with only a single zero disk fraction point (Per OB2), our results in Table 3 show about half of the target clusters with a zero disk fraction (Fig. 3). Because the number of IM stars for each cluster is typically more than 20, a simple stochastic effect due to a small number of stars is not likely to be the reason for the many zero disk fraction points.

As a result of the fitting, the lifetime for the IM stars is found to be significantly shorter than that for the LM stars. The above results are summarized in Table 4. In the case of fitting, including the upper limits (survival fitting), the estimated lifetime ($t_{\text{IM},JHK}^{\text{life}} = 2.8 \pm 2.4$ Myr), is much shorter than that of the LM stars ($t_{\text{LM},JHK}^{\text{life}} = 9.7 \pm 1.1$ Myr) by about 7 Myr. These results clearly show the existence of a stellar mass dependence for the lifetime of the innermost disk.

6.3 Stellar mass dependence of the disk lifetime

The stellar mass dependence of the disk lifetime can be a strong constraint on the disk dispersal mechanism and the theory of planet formation, as discussed by Kennedy & Kenyon (2009). They compared the disk fraction for different mass bins, $\sim 1 M_{\odot}$ (0.6–1.5 M_{\odot}) and $\sim 3 M_{\odot}$ (1.5–7 M_{\odot}), in seven clusters and suggested that their data are more consistent with $\tau_{\text{KK09}} \propto M_*^{-1/2}$ than with $\propto M_*^{-1/4}$. τ_{KK09} is the disk decay time-scale defined by their model, in which the disks are dispersed when the accretion rate drops below the wind-loss rate. However, only four clusters appear to be the main contributors to the resultant mass dependency (see fig. 9 in Kennedy & Kenyon 2009) – the H α disk fraction for three clusters and the MIR disk fraction for one cluster. Although Hernández et al. (2005) and Carpenter et al. (2006) found similar stellar mass dependence for clusters

with ages >3 Myr, the dependence is uncertain because of an insufficient number of clusters, in particular those with ages ≤ 3 Myr. Obviously, it is necessary to increase the number of data points to clarify the mass dependence. Also, the large uncertainty in previous studies might be the result of differences in the evolution of the *K* and MIR disks. Thus studying of only the *JHK* disk (or only the MIR disk) might show a clearer mass dependence.

The stellar mass dependence of the disk lifetime can be quantitatively estimated by combining the time-scales for the two mass ranges. For the IMDF, stars with mass of 1.5–7 M_{\odot} are used in this paper. Considering the larger number of lower-mass stars with the typical universal IMF (e.g. Kroupa 2002), the characteristic mass is set as 2–3 M_{\odot} , or 2.5 M_{\odot} . We estimated the stellar mass dependence with a characteristic mass from 2–3 M_{\odot} , but no significant difference was found within the uncertainties. The characteristic mass of $0.5 \pm 0.5 M_{\odot}$ (0.1–1 M_{\odot}) for the LMDF is set by considering the IMF and mass detection limit ($\sim 0.1 M_{\odot}$) for clusters used to derive disk fractions. Assuming the stellar mass dependence of the disk lifetime as a power-law function of stellar mass, we find $t_{JHK}^{\text{life}} \propto M_*^{-0.8 \pm 0.7}$ using the survival fitting. These results are tabulated in Table 4. Our result is consistent with the results by Kennedy & Kenyon (2009), who found τ_{KK09} is proportional to about $M_*^{-0.5}$. However, note again that our results are derived only from the *K*-disk data, while Kennedy & Kenyon (2009) used mostly data from the MIR disk or the H α gas disk. We discuss the difference of disk lifetimes of the *K* disk, MIR disk, and gas accretion disk in § 8.

7 EVOLUTION OF THE MIR DISK

In this section, we discuss the evolution of the inner disk of IM stars traced by the MIR excess emission and using the results on the MIR IMDF derived in Section 4.

7.1 Disk lifetime

In Fig. 4, we plot the MIR IMDFs, showing a relatively clear exponential decay curve from cluster age zero to ~ 10 Myr. We performed fitting in the same way as for the *K* disks (Section 6). By including the upper limits (two clusters: NGC 2362 and γ Vel), a survival analysis was performed to obtain $\tau = 2.3 \pm 1.4$ Myr and $\text{DF}_{0(\text{MIR})}$ of 73 ± 57 per cent, which leads to a disk lifetime of $t_{\text{IM,MIR}}^{\text{life}} = 6.1 \pm 4.2$ Myr. The resultant fitted line is shown with the black line in Fig. 4. The fitted results are consistent with a 100 per cent initial disk fraction for the MIR IMDF.

7.2 Comparison with low-mass stars

We also plot the MIR LMDF for comparison in Fig. 4. The data points for MIR LMDFs are for 18 clusters from *Spitzer* observations: 16 clusters in Roccatagliata et al. (2011)⁴ and Orion OB1bc and Orion OB1a/25 Ori in Kennedy & Kenyon (2009). We performed fitting in the

⁴ For the LMDF, we excluded two clusters from their 18 target clusters. First, NGC 2244 is excluded because the detection limit

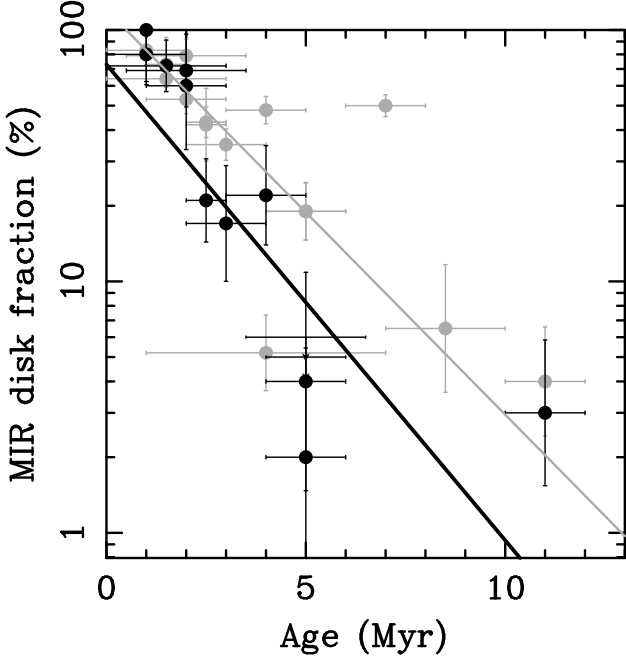


Figure 4. MIR IMDF (black) and MIR LMDF (gray) of young clusters in the solar neighborhood as a function of cluster age. For the IMDF, the data for clusters in Table 3 are shown with black filled circles, while upper-limits are shown with downward arrows (only two clusters at 5 Myr, NGC 2362 and γ Vel). The fitted curve using survival analysis for all the data including the upper limits is shown with the thick black line. The fitting for the LMDF is shown with the gray line.

same way as in Section 6 to obtain $t_{\text{LM,MIR}}^{\text{life}} = 8.6 \pm 0.7$ Myr and $\text{DF}_{0(\text{MIR})} = 120 \pm 12$ per cent with a reduced χ^2 value of 1.0 with a degree of freedom of 16. This result is consistent with 100 per cent initial disk fraction for the MIR LMDF. There is no significant difference in the disk fraction lifetime between the IMDF and LMDF disk, unlike for the K disk in the previous section.

7.3 Stellar mass dependence of the disk lifetime

The results of the lifetimes for the MIR disks of both IM and LM stars are summarized in Table 4. We derived the stellar mass dependence of the MIR disk lifetime as $t^{\text{life}} \propto M_*^{-0.2 \pm 0.3}$, assuming a power-law function and using the characteristic masses for the two mass ranges as for the JHK disk lifetime (Section 6.2) and the results for the survival fitting. These results are tabulated in Table 4.

Our results show no significant stellar mass dependence of the disk lifetime, which is apparently inconsistent with Kennedy & Kenyon (2009), who derived a steeper stellar mass dependence of $\tau_{\text{KK09}} \propto M_*^{-0.5}$. However, note that their results are based on the lifetime of both dust and gas disks. The strong dependency appears to be mainly contributed from the inclusion of $\text{H}\alpha$ gas disk. They suggested a $M_*^{-0.5}$ dependence rather than $M_*^{-0.25}$ dependence mostly

based on the data for three clusters (Taurus ($\text{H}\alpha$), Tr 37 ($\text{H}\alpha$ & MIR), and OB1bc ($\text{H}\alpha$); see their fig. 9), but the existence of the disks is based mostly on the $\text{H}\alpha$ gas disk for those three clusters. Using their data, we attempted to estimate the mass dependence and confirmed that $\tau \propto M_*^{-0.5}$ is obtained in the case of using only the $\text{H}\alpha$ disk fraction for the eight clusters in their list except for OB1a/25Ori, while $\tau \propto M_*^{-0.2}$ is obtained in the case of using only the MIR disk fraction for the same eight clusters. Therefore, we conclude that there is no mass dependence of the lifetime of an MIR disk within the uncertainties.

8 DIFFERENCE IN THE EVOLUTION OF K AND MIR DISKS

In the previous sections, we discussed the disk lifetime of the K disk, which traces the innermost dust disk, and the MIR disk, which traces the inner disk outside of the K disk. In this section, we compare the K and MIR disk fractions and discuss the evolution of the K disk and the MIR disk. We also discuss the relation of the MIR disk to the inner *gas* disk, which is traced by accretion signatures, such as the $\text{H}\alpha$ emission line.

8.1 Comparison of the K disk and the MIR disk

8.1.1 Low-mass stars

Before discussing the case for the IM stars, we take a look at the case for the LM stars as a reference. Fig. 5 (right) shows the comparison of the JHK LMDF (red) and the MIR LMDF (blue). The derived lifetime for the K disk (9.7 ± 1.1 Myr) and the MIR disk (8.6 ± 0.7 Myr) are identical within the uncertainties (see Table 4), which suggests that the K disk and the MIR disk disperse almost simultaneously in the disks of LM stars. This is consistent with the recent view of disk dispersal that the *entire* disk disperses almost simultaneously for low-mass stars ($\Delta t \lesssim 0.5$ Myr; Andrews & Williams 2005).

8.1.2 Intermediate-mass stars

We compared JHK and the MIR IMDFs in Fig. 5 (left). The filled circles showing IMDFs and the arrows showing upper limits are labeled with the cluster numbers in Table 1. This figure immediately suggests that the MIR IMDFs are systematically larger than the JHK IMDFs. The MIR IMDF appears to be almost as high as 100 per cent at $t \sim 0$ and exponentially declines, while the JHK IMDF is less than 50 per cent at the beginning and keeps smaller values than the MIR IMDF throughout the age span. Because this offset might be due to an incomplete cluster sampling that favors only the higher MIR or the lower JHK IMDFs, we directly compared the MIR and JHK IMDFs for the clusters that have both fractions estimated. The results (see Figure 6) show that the MIR IMDFs are systematically larger than the JHK IMDFs for all the 13 clusters that have both. We thus conclude that the large offset of the IMDFs is real, and that the smaller JHK IMDF is a unique property of the IM stars disk lifetimes compared to those of the LM stars. The significantly lower disk fraction of the K disks means they

is not given. Second, γ Vel is excluded because the completeness limit for this cluster does not reach the low mass ($< 1 M_{\odot}$) limit.

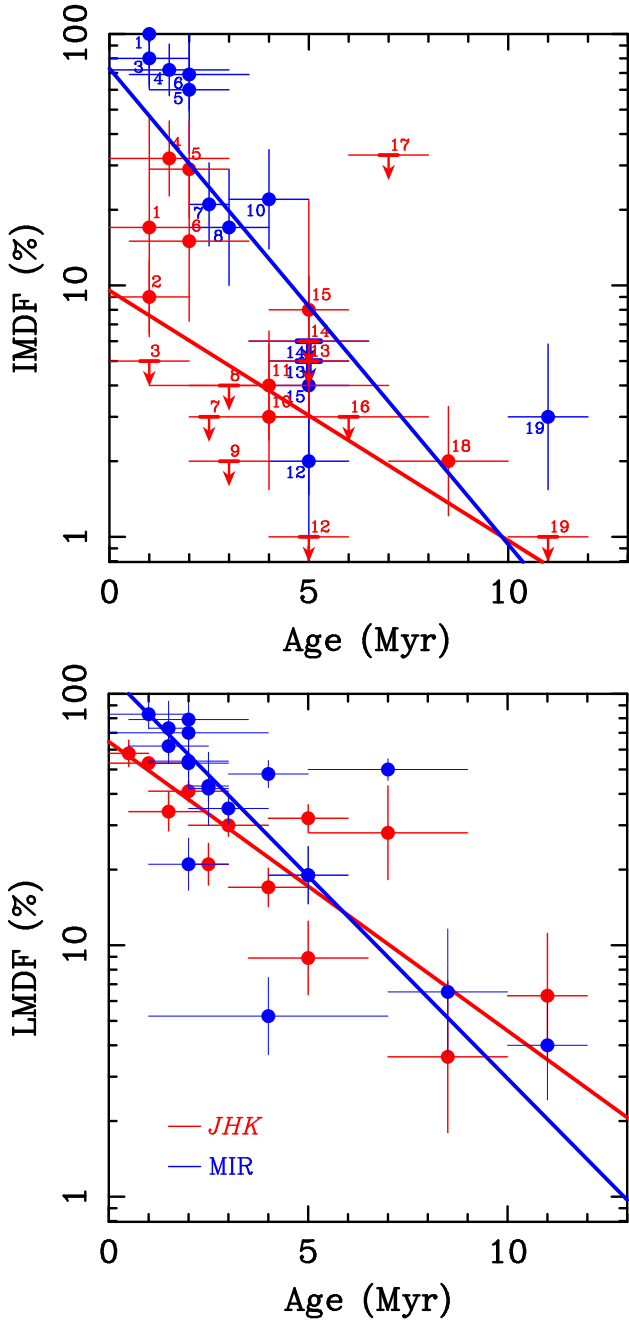


Figure 5. Comparison of *JHK* disk fraction (red) to *MIR* disk fraction (blue) as a function of cluster age. The left figure is for intermediate-mass stars (IMDF), while the right figure is for low-mass stars (LMDF). For the IMDF, the red filled circles show the *JHK* IMDF from Section 6 (Table 3), while the blue filled circles show the *MIR* IMDFs from the same table. The arrows show the upper limits. Both circles and arrows are labeled with the cluster numbers in Table 1. The lines show the fits with survival analysis including the upper limits. For the LMDF, red filled circles are from Yasui et al. (2009, 2010), while blue filled circles are mainly from Roccatagliata et al. (2011) (see the text for the details).

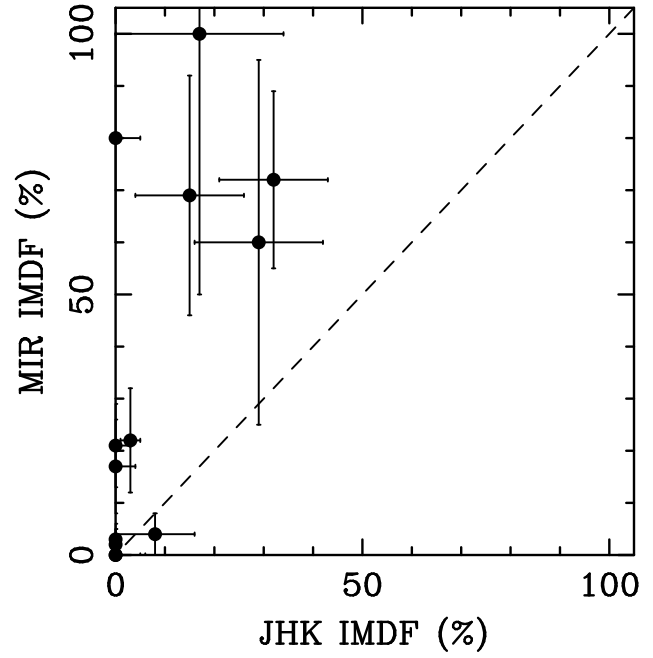


Figure 6. Comparison of *JHK* IMDF to *MIR* IMDF for 13 target clusters for which both *JHK* and *MIR* IMDFs are available (see Table 3).

disappear much *earlier* than the *MIR* disks. The lifetime difference is about 3 Myr ($6.1 - 2.8 = 3.3$ Myr; see Table 4).

As suggested in section 2.2, possible contamination of LM stars in selecting IM stars may affect the above discussion. Therefore, it is safer to set the lower limit mass for IM-stars as $2 M_{\odot}$, which is slightly larger than the nominal mass limit in this paper ($1.5 M_{\odot}$). With this lower limit mass, we derived the *JHK*/*MIR* IMDFs in the same way as in section 2, 3, and 4. As a result, the derived IMDFs do not largely differ, and the estimated lifetimes of *K*- and *MIR*-disk are 2.7 ± 3.6 Myr and 6.0 ± 6.1 Myr, respectively, which are very close to the results for the lower mass limit of $1.5 M_{\odot}$ although the uncertainties for both disk fractions and disk lifetimes become larger. Therefore, we conclude that the effect of possible contamination of LM stars to our IM-star samples is very small, and that it does not change the conclusion.

An alternative approach was tried to confirm these results. To increase the statistical significance, we binned all of the disk-harboring stars and cluster members in the cluster age range from 1 to 5 Myr with 1 Myr bins and 1 Myr steps and computed both the *JHK* and *MIR* IMDFs. To have enough clusters, all the members of the four clusters in the 6 to 11 Myr range are accumulated to estimate a binned IMDF at 8.5 ± 2.5 Myr for the *JHK* IMDF. Because we have only one data point at $t = 11$ Myr for the *MIR* IMDF, we simply used it without binning. This ‘binning’ process effectively reduces the number of upper-limit points, and the disk fraction curve becomes clearer with less scatter.

The results are plotted in Figure 7, which suggests the disk fraction offset between the *JHK* and the *MIR* IMDFs as well as the lifetime difference. The fitting results for the *JHK* IMDFs are as follows: disk lifetime ($t_{\text{IM}, \text{JHK}}^{\text{life}}$) of 3.3 ± 0.9 Myr with $\text{DF}_{0(\text{JHK})}$ of 35 ± 13 per cent with χ^2_{ν} of 1.0 with degree

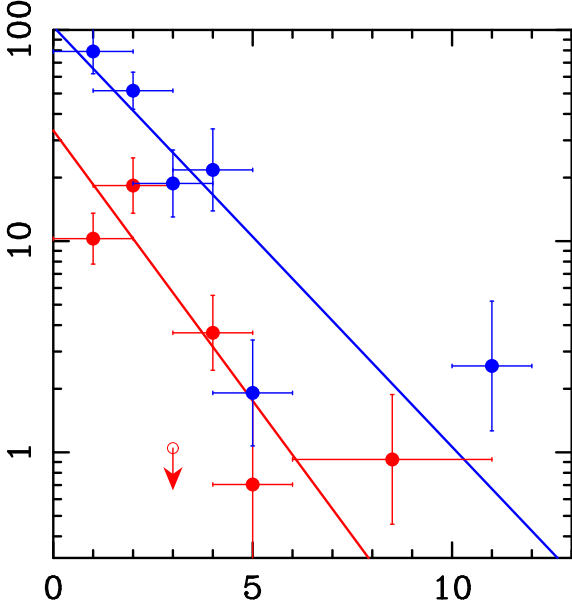


Figure 7. Comparison of the *JHK* IMDF (red) to the *MIR* IMDF (blue) as a function of age. Same as the left figure of Figure 5, but the data are binned in the age axis direction (see Section 8.1 for details). The straight lines show the fits to the data points with the upper limit at 3 Myr excluded from the fitting of *JHK* IMDF.

of freedom of 3. The derived lifetime is, in fact, very close to the results without binning (2.8 Myr). Note that the data point at $t = 3$ Myr was not used because it remains an upper limit due to many upper limits in this age bin. As for *MIR* IMDF, a disk lifetime ($t_{\text{IM,MIR}}^{\text{life}}$) of 6.7 ± 1.1 Myr with $\text{DF}_{0(\text{MIR})}$ of 104 ± 26 per cent with χ^2_ν of 2.2 with degree of freedom of 4 were obtained. In summary, these ‘binning’ fitting results (see Table 4) confirm the survival analysis results without binning although there are very few data points in the binning fitting and we should be cautious of any unknown biases. The stellar mass dependence for this binning analysis is also listed in Table 4 and is consistent with previous results. Therefore, we conclude that there is a lifetime difference of ~ 3 –4 Myr between *K* and *MIR* disks.

8.2 Comparison with the submm disk

To investigate further the dependence on stellocentric distance, we also compared the disk fraction and lifetime of the *K* and *MIR* disks with that of the outer cold (~ 10 K) dust disk traced by the submm and mm continuum. There are a number of studies of submm observations of IM stars in Taurus (1.5 Myr), ρ Oph (2 Myr), and Upper Sco (5 Myr) (Andrews & Williams 2005, 2007; Mathews et al. 2012). We confirmed that the *MIR* disk is well correlated with the submm disk for the IM stars. Out of the observed 20 B-, A-, F-, and G-type stars in the above papers, 19 stars are detected with *MIR* and submm disks, and only one star, HIP 76310 in Upper Sco, lacks a *MIR* disk but has a submm disk. The strong correlation clearly suggests that the *MIR* inner disk and submm outer disk disperse almost simultaneously for the IM stars. This behaviour is similar to that for LM stars (Andrews & Williams 2005, 2007; Mathews et al.

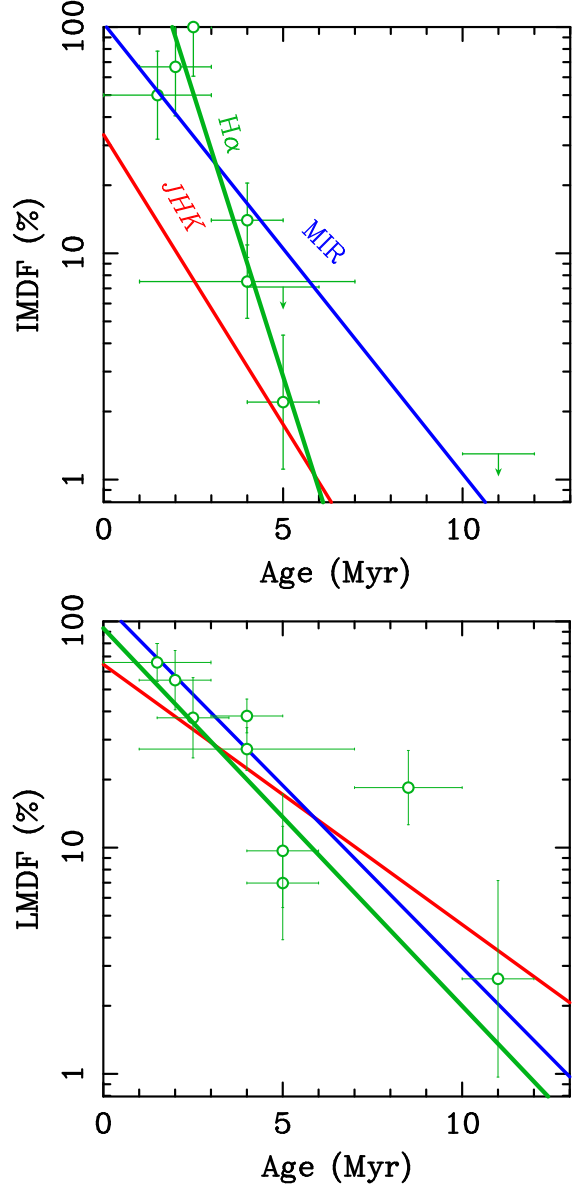


Figure 8. Comparison of disk fraction curves of the *K* disk (red line), *MIR* disk (blue line), and $\text{H}\alpha$ disk (green line). For the *JHK* and the *MIR* IMDFs, the binned fitting results are shown (see Section 8.1.2). The $\text{H}\alpha$ disk fraction from Kennedy & Kenyon (2009) is plotted with open circles. The left figure is for the IMDF, while the right figure is for the LMDF.

2012). Thus the early disappearance of the innermost *K* disk again appears to be the only unique property of the IM stars compared to the LM stars.

8.3 Comparison with the $\text{H}\alpha$ gas disk

Another question we investigated is how the dust disk evolution is synchronized with the *gas* disk evolution. We compared the disk fraction and lifetime of the *K* and *MIR* disks with those of the innermost gas disk traced by the $\text{H}\alpha$ emission as has been comprehensively studied by Fedele et al. (2010). They used spectroscopy of the $\text{H}\alpha$ emission for the clusters in the solar neighbourhood. Because the $\text{H}\alpha$ emis-

sion was not observed for many IM stars, we used the $H\alpha$ disk fractions from Kennedy & Kenyon (2009) (their 1.5–7 M_{\odot} samples for IMDF and all mass range samples for LMDF) and directly compared them with those of K and MIR disks. This is shown in Fig. 8. The left panel includes eight clusters (Taurus, Cha I, IC 348, Tr 37, Ori OB1bc, Upper Sco, NGC 2362, and NGC 7160), and the right panel includes an additional cluster (OB1a/25Ori).

In the right panel of Fig. 8, the $H\alpha$ LMDF closely traces JHK and MIR LMDFs, and this shows the co-evolution of the dust and gas disks for LM stars. This is consistent with the results of Fedele et al. (2010), who found that the time-scale of $H\alpha$ mass accretion is almost the same as that of the dust disk. In the left figure, however, the $H\alpha$ IMDF shows a different cluster age dependence compared to the IMDF of the dust disk. We note that (1) it overlaps the MIR IMDF at younger ages (<5 Myr), and (2) it is systematically larger than the JHK IMDF at younger ages with a longer lifetime than the K disk. While the first point suggests the co-evolution of the gas and dust disk, which is suggested by Fedele et al. (2010), the second point has not been noted before. Only the K disk appears to have a unique cluster age dependence among the different disk components of the IM stars.

8.4 Long transition disk phase for IM stars

In summary, for the IM stars there appears to be the following lifetime sequence for the various stellocentric radii: $t_K^{\text{life}} < t_{H\alpha}^{\text{life}} \lesssim t_{\text{MIR}}^{\text{life}} \sim t_{\text{submm}}^{\text{life}}$. On the other hand, all these time-scales are nearly the same for the LM stars (Andrews & Williams 2005, 2007; Mathews et al. 2012). The above result suggests that for the IM stars the K disk has a shorter time-scale and an evolutionary history that is different from that of the LM stars. The observed longer lifetime with larger stellocentric distance is qualitatively consistent with the recent view of the disk dispersal sequence for protoplanetary disks of LM stars (Williams & Cieza 2011). However, the lifetime difference between the K and MIR disks for the IM stars ($\sim 3\text{--}4$ Myr) is significantly longer than that suggested previously for low-mass stars ($\Delta t \lesssim 0.5$ Myr; e.g. Williams & Cieza 2011).

That a time lag is clearly seen *only for the IM stars* gives us a clue to the mechanism of disk evolution. The time-lag between K - and MIR-disk lifetimes can be interpreted as a *transition disk phase*, in which the innermost K disk disappears while the outer MIR disk remains. Disks with no JHK excess emission and with MIR excess are called ‘classical’ transition disks (Muzerolle et al. 2010), while the original definition of ‘transition disk’ is a disk that has no or little excess emission at $\lambda < 10 \mu\text{m}$ and a significant excess at $\lambda \geq 10 \mu\text{m}$ (Strom et al. 1989; Wolk & Walter 1996). The two significant processes, disk dispersal (e.g. Muzerolle et al. 2010) and planet formation (e.g. Calvet et al. 2002), are thought to happen during this phase. Therefore, our finding suggests that such critical evolutionary events can be clearly recognized in the transition disk phase for IM stars as a time lag between the dispersal of the K disk and the dispersal of the MIR disk, while both events happen nearly simultaneously for the LM stars ($\Delta t \lesssim 0.5$ Myr).

9 PHYSICAL MECHANISM OF THE DISK EVOLUTION OF INTERMEDIATE-MASS STARS

In this section, we discuss the implications of the observed time-scales of the gas/dust disks on the mechanism of disk evolution of the IM stars. Although there are many detailed processes related to disk evolution, we focus on discussing the following two categories, which are not intended to be comprehensive but broadly cover basic processes related to disk evolution: (1) the disk dispersal processes, such as mass accretion and dissipation by photoevaporation, and (2) the dust settling to the disk midplane and dust growth, which could be connected to planetesimal formation and planet formation. We suggest that the latter process is more likely for the early disappearance of the K disks.

Before discussing the detailed evolution mechanisms, we first remark on the radial configuration of the dust disk in the steady state. If we consider an optically thick disk for disks with IR excess, the radius (R) with a temperature (T) is given by $R = (L_*/4\pi T^4 \sigma)^{1/2}$, where L_* is the stellar luminosity and σ is the Stefan-Boltzmann constant. The dust temperature is about 1500 K for the K disk and ~ 500 K for the MIR disk as inferred from the peak wavelength of the black body emission. From those typical temperatures, the stellocentric distances to those disks regions are estimated to be $r_K \sim 0.3$ AU, $r_{\text{MIR}} \simeq 5$ AU for IM stars (with the characteristic mass $M_* \sim 2.5 M_{\odot}$) and $r_K \simeq 0.1$ AU, $r_{\text{MIR}} \simeq 1$ AU for LM stars (with the characteristic mass $M_* \sim 0.5 M_{\odot}$) (see Fig. 9), considering the effective temperatures of the central star (see Millan-Gabet et al. 2007). Because the radius R of an optically thick disk with IR excess is expressed with $R = (L_*/4\pi T^4 \sigma)^{1/2}$, R is proportional to M_*^2 with the mass-luminosity relation of $L_* \propto M_*^4$ (Siess et al. 2000). Therefore, r_K and r_{MIR} should be roughly proportional to M_*^2 .

9.1 Disk dispersal?

The disk dispersal process consists of two kinds of processes: *mass accretion* onto the central star and *dissipation* into interstellar space (Hollenbach, Yorke & Johnstone 2000). The combination of mass accretion and dissipation due to photoevaporation (e.g. the so called ‘UV-switch model’; Alexander 2008) is thought to be one of the major mechanisms of overall disk dispersal (Williams & Cieza 2011), because this can explain the almost simultaneous dispersal of the entire disk ($\Delta t \lesssim 0.5$ Myr), and thus the short transition disk phase as implied in Fig. 8 (right). Although there are a number of other proposed dispersal mechanisms (e.g. stellar encounter, disk wind), our discussion here focuses on the dispersal due to photoevaporation.

9.1.1 Accretion onto the central star?

The first possible mechanism for the short K -disk lifetime of the IM stars is the faster mass accretion onto the central star for higher-mass stars. Mendigutía et al. (2011) suggested a very strong mass dependence of the mass accretion rate from observations of UV Balmer excess. However, our results suggest that the gas accretion disk has a longer lifetime than the K disk (Fig. 8, left), about equal to that of the MIR

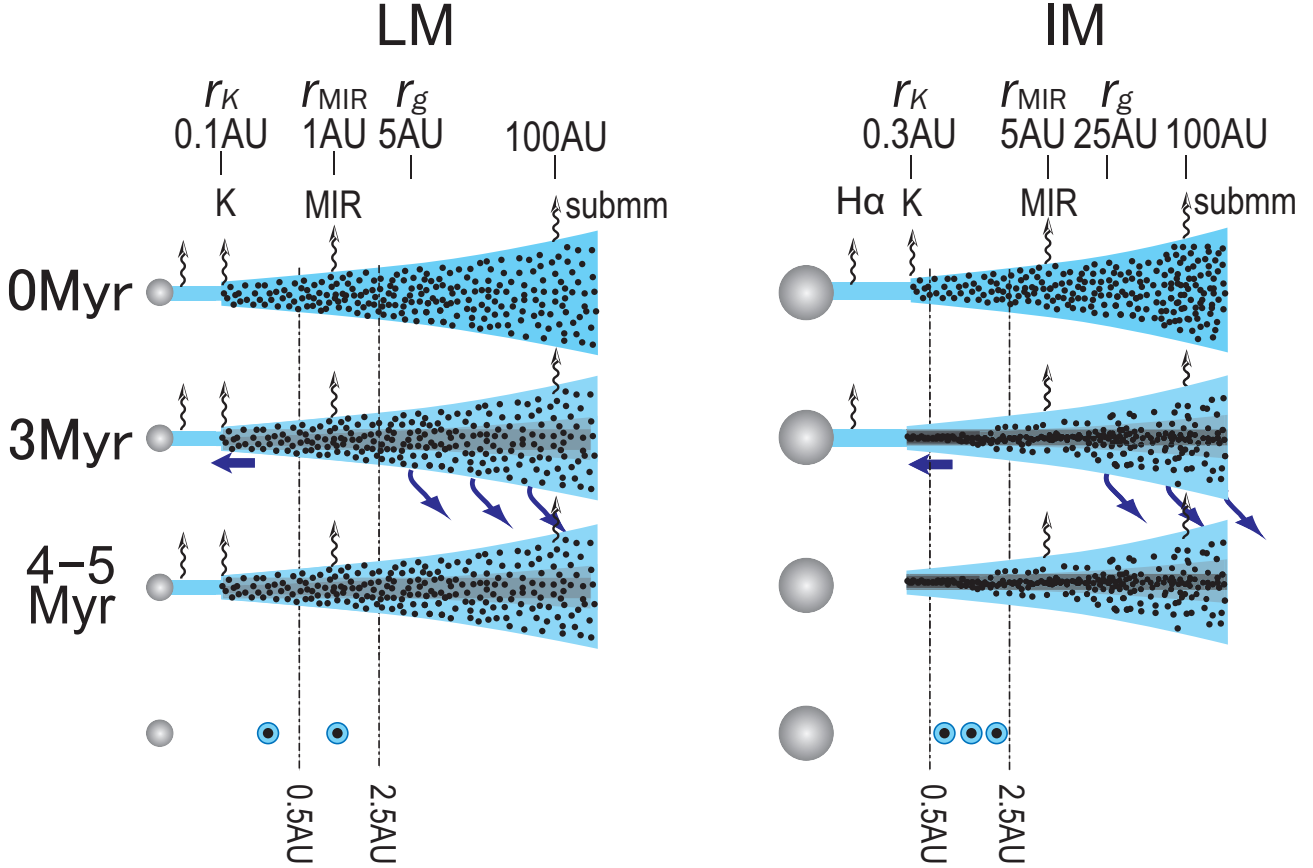


Figure 9. Proposed disk evolution sequences for LM stars (left) and IM stars (right) as discussed in Section 9. The radius in the horizontal direction is roughly shown with a logarithmic scale. r_K , r_{MIR} , and r_g denote the K-disk radii, MIR-disk radii, and photoevaporation radii, respectively. Blue arrows show the dispersal of gas/dust. Black dots and the cyan region show the dust and gas distribution, respectively, while Jupiter-mass planets are shown by circles with cyan and black. K, MIR, submm, and H α emissions are shown by arrows with wavy lines. After 4–5 Myr, the entire gas/dust disk disperses before the dust settling is completed for LM stars (left), while the entire gas/dust disk disperses *after dust settling is completed in the K disk* for IM stars (right). After the dispersal, the Jupiter-mass planets are left (bottom). It is known that a larger number of Jupiter-mass planets are distributed at < 2.5 AU for IM stars than for LM stars). The thin vertical lines at $r = 0.5$ AU show the inner region where close-in planets are rarely found for IM stars (see Section 9.3). Note that this is intended to describe the typical case and is not applicable to all stars.

disk. Therefore, more rapid accretion and the resultant deficiency of material are not likely to be the cause of the faster destruction of the K disk.

9.1.2 Photoevaporation?

Photoevaporation is another strong candidate for the dispersal mechanism that may cause the short K-disk lifetime. Photoevaporation is known to be effective for outside of the gravitational radius, r_g , where the thermal energy balances with gravitational potential. This radius scales with the stellar mass as $r_g \sim GM_*/c^2$ (Alexander 2008), and r_g for IM stars ($2.5 M_\odot$) and LM stars ($0.5 M_\odot$) are ~ 25 AU and ~ 5 AU, respectively. The corresponding K disk radii (r_K) for IM and LM stars are only ~ 0.3 and ~ 0.1 AU, respectively, which are less than $1/50$ of r_g . Similarly the corresponding MIR disk radii are ~ 5 and ~ 1 AU, respectively. Although all these radii change with the stellar mass (from 1.5 to $7 M_\odot$ for IM stars), the relative magnitude of the radii, $r_K < r_{\text{MIR}} < r_g$, should not change for both IM

and LM star mass ranges, even considering the scaling with the stellar mass mentioned above. Therefore, photoevaporation is not likely the main cause of the fast K-disk dispersal for IM stars.

9.2 Dust settling, dust growth, and planet formation

The transition disk phase is now interpreted as the most important phase in the standard planet formation scenario, and now much observational effort has been put into characterizing this phase (Williams & Cieza 2011). In this interpretation, the early disappearance of the innermost dust disk compared to other portions of disk is due to dust settling to disk mid-plane (Kenyon & Hartmann 1987; Dullemond & Dominik 2005) and/or dust growth (Weidenschilling 1997; Dullemond & Dominik 2004). We discuss those possibilities in the following section with a schematic picture shown in Fig. 9.

9.2.1 Dust settling & growth

From the basic equations of protoplanetary disks in equilibrium, the radial dependence of the dust settling time can be analytically shown to be proportional to the Kepler rotation period, which is proportional to $r^{3/2} M_*^{-1/2}$ (Nakagawa et al. 1981). Although there are many new simulations incorporating more physical processes to show the dust settling time with a different r - or M_* -dependence (e.g., Tanaka, Himeno, & Ida 2005), we compare our results with this base relationship by Nakagawa et al. (1981) as an initial consistency check.

First, as for the radius r dependence, the shorter K -disk lifetime than that of MIR-disk for the IM stars (Fig. 9, right, Table 4) is qualitatively consistent with the base relationship in that the dust settling/growth is occurring more effectively in the inner disk. Although the observed results ($t_{\text{life}}^{\text{K}} \sim 3$ Myr at $r_K \sim 0.3$ AU, and $t_{\text{life}}^{\text{MIR}} \sim 6$ –7 Myr at $r_{\text{MIR}} \sim 5$ AU) do not quantitatively follow the base $r^{3/2}$ relation and instead show a much weaker r -dependence, this can be interpreted as that the turbulent process or some other processes that prevent the dust settling/growth have the opposite r -dependence to reduce the r -dependence of dust settling/growth (e.g., Dullemond & Dominik 2005). For the LM stars, on the other hand, the lifetimes of the inner K , MIR, and the outer submm disks do not show any significant difference (see discussions in Section 8.1.1 and 8.2). This is even more inconsistent with the base $r^{3/2}$ relation than the IM stars. Most likely this means that the disk disperses before dust is totally settled in the entire disk, although dust settling/growth is reported for some LM stars (e.g., Pinte et al. 2008). In this case, the dust in the upper disk layer is dissipated in the process of mass accretion and photoevaporation (Fig. 9, left), and the disk lifetime (~ 9 –10 Myr) sets the lower limit of the dust setting/growth time-scale for most of the LM stars. However, it should be noted that the above discussion is intended to describe the typical case and is not applicable to all stars. The time scale of transition disk is still under debate, short (~ 0.2 Myr; e.g. Luhman et al. 2010) or long (\sim a few Myr; e.g. Sicilia-Aguilar & Currie 2011), although the discrepancies among these studies are largely due to differing definitions of the transition disk and how to estimate the total disk lifetime (Espaillet et al. 2014).

Next, as for the stellar mass M_* dependence, the much shorter K -disk lifetime of the IM stars than that of the LM stars ($t_{\text{IM},JHK}^{\text{life}} \sim 3$ Myr, while $t_{\text{LM},JHK}^{\text{life}} \sim 9$ –10 Myr; see Table 4; Fig. 5, left) is apparently consistent with the base relation in that dust settling/growth occurring effectively for higher-mass stars. However, if we also consider the r -dependence, the characteristic IM stars ($M_* = 2.5 M_\odot$, $r_K = 0.3$ AU) are expected to have longer settling time-scale (about twice) than the characteristic LM stars ($M_* = 0.5 M_\odot$, $r_K = 0.1$ AU) which shows the opposite tendency compared to the observed timescales. This might suggest that turbulence of the innermost disk is much weaker for the IM stars than for the LM stars so that the dust growth/settling occurs quickly. Although the larger disk mass (surface density) for stars with higher mass (Andrews & Williams 2005) might cause such a situation, the physical process is unknown.

9.2.2 Planet formation

Planetesimal and planet formation result from the dust settling/growth processes according to the standard core-accretion model (Lissauer & Stevenson 2007). For IM stars, the quick dust settling/growth processes in the presence of gas may cause effective planetesimal formation (Hubickyj et al. 2005). This results in effective Jupiter-mass planet formation (e.g. Laughlin et al. 2004; Ida & Lin 2004a; Robinson et al. 2006), which could accelerate the disappearance of the innermost disk with clearing by migration (Lin, Bodenheimer & Richardson 1996; Trilling et al. (1998); Trilling et al. (2002)). Such a scenario is consistent with the trend of a higher probability of Jupiter-mass planets with a larger stellar mass for stars in the mass range of 0.2 – $1.9 M_\odot$ for semimajor axes of <2.5 AU (Johnson et al. 2010). However, the mass range for IM stars (1.5 – $7 M_\odot$) has only a small overlap with this trend. This trend is generally interpreted as a result of larger disk mass (high surface density) for larger stellar mass, which enables the rapid formation of Jupiter-mass planets (e.g. within 1 Myr; Ida & Lin 2004b).

9.2.3 Summary

In summary, dust settling/growth (and some planet formation) can generally explain the shorter K -disk lifetime of IM stars, although the specific physical processes are not known. This interpretation is summarized in the schematic pictures shown in Fig. 9 (right): (1) The K disk ($r_K \sim 0.3$ AU): Dust settling/growth works very efficiently from the beginning of disk evolution (cluster age = 0) and is almost completed in ~ 3 Myr. Because there is no left-over IR-emitting grains even in the upper disk layer, no NIR continuum is emitted, (2) The MIR disk ($r \sim 5$ AU): A significant amount of dust grains are in the upper disk layer due to the turbulence and give rise to the MIR continuum emission. After ~ 4 –5 Myr, dust settling has occurred, or dust in the upper layer of the MIR disk is dissipated, resulting in no emission of MIR–thermal continuum emission. If this picture is correct, the lifetime difference of JHK and MIR IMDFs constrains the time-scale of this settling process in the K disk to about ~ 4 Myr (Section 8.1.2) (Table 4). The low initial value of the JHK IMDF ($\sim 50\%$) might also be naturally explained with the effective settling in the inner disk. Future MIR spectroscopy of the silicate emission lines and the SED slope (Furlan et al. 2006) of those IM stars with and without the K disk will test the idea that the disappearance of the K disk is due to dust settling/growth.

10 IMPLICATIONS FOR PLANET FORMATION AROUND IM STARS

Two remarkable trends are known for the Jupiter-mass planets around IM stars: (1) the lack of close-in planets with semimajor axes of $\lesssim 0.5$ AU orbiting stars with masses $M > 1.5 M_\odot$ (such planets are common for stars with $M_* < 1.2 M_\odot$), and (2) the higher probability of having planets with semimajor axes of <2.5 AU compared to low-mass stars. In this section, we discuss these trends in the context of our disk fraction lifetime results.

10.1 Implications for the lack of close-in planets

There appears to be a lack of close-in planets with semi-major axes of $\lesssim 0.5$ AU orbiting stars with masses of $1.5\text{--}3 M_{\odot}$ in planet-search surveys, while close-in planets are more frequent for lower-mass stars (Wright et al. 2009). Because planets are thought to form in situ or migrate inward in the formation phase (e.g. Lin et al. 1996), our suggestion of rapid planet formation in the K disk appears to be inconsistent with the paucity of close-in planets. However, considering the possible radial range of ‘ K disk’ (from ~ 0.3 AU to 1 AU, depending on the mass of the central star, disk mass, etc.), the higher planet occurrence for higher-mass stars (Johnson et al. 2010) may reflect the rapid planet formation at $r \gtrsim 0.5$ AU. The planets that formed at $r \lesssim 0.5$ AU may have dropped into the central stars due to migration (Papaloizou et al. 2007) because the gas disk traced by $H\alpha$ still remains for about 2 Myr after the disappearance of the K disk. Or, they may have disappeared due to collisional destruction that may have effectively occurred along with grain growth (Johansen et al. 2008). In any case more studies are necessary to understand the precise relation between disk lifetime and planet formation.

Regarding the lack of close-in planets for IM stars, two major scenarios have been proposed. The first scenario is planet engulfment caused by the stellar evolution of primary stars in the RGB phase (Villaver & Livio 2009). Another scenario is that the observed differences in orbital distribution are primordial, and they are a consequence of the planet-formation mechanism around the more-massive stars (Currie 2009). In this section, we focus on the latter scenario because our results are relevant to the early stages of star formation. Currie (2009) suggests that planets around IM stars cannot migrate to inner orbits because of the shorter gas-disk lifetime for IM stars. In addition, Kretke et al. (2009) suggest that the inner edge of the dead zone in protoplanetary disk, where the dead zone is the region of the disk without magnetorotational instability (Gammie 1996), effectively determines the semimajor axes of giant planets because the dead zone traps inwardly migrating solid bodies. Thus, they suggested that the larger radius of the inner edge for higher mass stars explains the lack of close-in planets.

Our results are qualitatively consistent with Currie’s scenario in that shorter disk lifetimes are expected for higher-mass stars. We estimated that the stellar mass dependence of gas disk lifetime $t_{H\alpha}^{\text{life}}$ is about $M_*^{-0.5}$ ($t_{\text{IM}, H\alpha}^{\text{life}} \sim 5$ Myr and $t_{\text{LM}, H\alpha}^{\text{life}} \sim 10$ Myr in Fig. 8). However, this dependence is not as steep as assumed in Currie (2009), $t_{\text{gas}}^{\text{life}} \propto M_*^{-\beta}$ with $\beta = 0.75\text{--}1.5$. In any case, migration alone may not be able to explain the observed sharp outward step in giant planet orbits as pointed out in Kennedy & Kenyon (2009).

Our results that the innermost disks of IM stars disappear at a very early time also seem to be consistent with Kretke’s dead zone model. Kretke et al. (2009) assumed a smooth stellar mass dependence of the inner edge radius of the dead zone (proportional to M_*) from the theoretical relationship between the radius and the mass accretion, and they compared this to the mass accretion rate derived from observations. Our results, showing the early disappearance of the innermost K disk, suggest that the radius becomes even larger because of low opacity, which makes the forma-

tion of dead zone difficult. If the critical stellar mass where the time lag between the K disk and the MIR disk dispersal is observationally determined, then this dead zone idea may be able to explain the lack of close-in planets even for the sharp cut-off at 0.5 AU in the planet semimajor axes in the distribution of Jupiter-mass planets.

In addition, the difference in the planet formation site in disks of IM stars and LM stars may explain the lack of close-in planets for the IM stars. Planets are thought to form outward of the snow line, ~ 3 AU for LM stars and ~ 10 AU for IM stars (Kennedy & Kenyon 2008). This difference might explain the observed difference in planet location even after the smearing out by the migration processes, although this idea does not explain the sharp step in planet semimajor axes.

10.2 Implications for higher planet formation probability

The probability of IM stars having Jupiter-mass planets is found to be proportional to $M_*^{1.0}$ for semimajor axes $< 2.5 M_{\odot}$ (Johnson et al. 2010). This observed frequency is likely to be determined by two competing effects: the tendency of shorter disk lifetimes for more massive stars reduces the likelihood of giant planets forming (Butler et al. 2006), and the tendency of higher disk masses for more massive stars increases the probability of gas-giant planet formation (Wyatt, Clarke & Greaves 2007). In Kennedy & Kenyon (2009), the stellar mass dependence of disk lifetime is estimated using the $H\alpha$ disk and MIR disk fractions as $\tau_{\text{KK09}} \propto M_*^{-1/2}$, where τ_{KK09} is the disk decay time-scale defined by their model. However, from our results, the disk lifetime at $r \gtrsim r_g$ for IM and LM stars is not significantly different, and the stellar mass dependence of disk lifetime ($t_{\text{MIR}}^{\text{life}}$) is as small as $M_*^{-0.2}$. The disk mass is known from submm observations to be roughly proportional to the stellar mass (Andrews & Williams 2005). The stellar mass dependence of the disk lifetime is negative, while the stellar mass dependence of the disk mass is positive. Therefore, the higher probability of IM stars having planets compared to LM stars seems to be due to the difference in disk mass instead of the difference in disk lifetime.

11 CONCLUSION

We derived and compiled protoplanetary disk fractions of intermediate-mass stars ($1.5\text{--}7 M_{\odot}$) for a large number of nearby young clusters (within 3 kpc and $\lesssim 5$ Myr old) with the available JHK photometric data in the literature. From the results and by comparing them with those for other wavelengths ($H\alpha$, MIR, and submm), we found the following results:

- The K -disk lifetime of IM stars (t_{JHK}^{life}), which is defined as the time-scale of disk fraction to bottom out at 5 per cent, is estimated to be 3.3 ± 0.9 Myr.
- The K -disk lifetime for the IM stars, t_{JHK}^{life} , is about one-third of that for the LM stars. Assuming a power-law dependence, the stellar mass dependence of the K -disk lifetime is found to be proportional to $M_*^{-0.7 \pm 0.3}$.

• By comparing the K disk ($r \sim 0.3$ AU) evolution to that of the MIR disk ($r \sim 5$ AU) for IM stars, we find that the K disk seems to disperse earlier than the MIR disk by ~ 3 – 4 Myr. Because the K disk and the MIR disk disperse almost simultaneously in LM stars ($\Delta t \lesssim 0.5$ Myr), the long time lag may be a characteristic of IM stars, suggesting that the transition disk is the common phase in IM stars.

• Because the disk time-scale at $r \gtrsim r_{\text{MIR}}$ for the IM stars does not seem to be significantly different from that of LM stars, the most likely cause for the time lag seems to be early dust growth/settling and/or Jupiter-mass planet formation in the innermost disk (K disk) in IM stars.

• Our results for the K disk of the IM stars suggest the possible reasons for the paucity of close-in planets around IM stars, but they are not conclusive. Our results also suggest that the disk mass is a more important factor for the stellar mass dependence of planet occurrence than the disk lifetime.

REFERENCES

- Adams F. C., Lada C. J., Shu F. H., 1987, *ApJ*, 312, 788
Alexander R., 2008, *New Astron. Rev.*, 52, 60
Andrews S. M., Williams, J. P., 2005, *ApJ*, 631, 1134
Andrews, S. M., Williams, J. P., 2007, *ApJ*, 671, 1800
Aspin, C., Sandell, G. 1997, *MNRAS*, 289, 1
Bessell M. S., Brett, J. M., 1988, *PASP*, 100, 1134
Briceño, C., Calvet, N., Hernández, J., Vivas A. K., Hartmann L., Downes J. J., Berlind P., 2005, *AJ*, 129, 907
Butler R. P., Johnson J. A., Marcy G. W., Wright J. T., Vogt S. S., Fischer D. A., 2006, *PASP*, 118, 1685
Caballero J. A., Albacete-Colombo J. F., López-Santiago J., 2010, *A&A*, 521, A45
Calvet N., D'Alessio P., Hartmann, L., Wilner D., Walsh A., Sitko M., 2002, *ApJ*, 568, 1008
Carpenter J. M., Mamajek E. E., Hillenbrand L. A., Meyer M. R., 2006, *ApJL*, 651, L49
Comerón F., Pasquali A., Figueras F., Torra J., 2008, *A&A*, 486, 453
Connelley M. S., Greene, T. P., 2010, *AJ*, 140, 1214
Cox A. N., 2000, *Allen's Astrophysical Quantities*. AIP Press, New York
Currie T., 2009, *ApJL*, 694, L171
Dahm S. E., 2008, in Reipurth, B. ed., *Handbook of Star Forming Regions, Volume I*. Astron. Soc. Pac., San Francisco, p. 966
Dahm S. E., 2008, in Reipurth, B. ed., *Handbook of Star Forming Regions, Volume II*. Astron. Soc. Pac., San Francisco, p. 26
Dahm S. E., Hillenbrand L. A., 2007, *AJ*, 133, 2072
Dullemond, C. P., Dominik, C., 2004, *A&A*, 417, 159
Dullemond C. P., Dominik C., 2005, *A&A*, 434, 971
Dullemond C. P., Dominik C., Natta A., 2001, *ApJ*, 560, 957
Elias J. H., 1978, *ApJ*, 224, 857
Elmegreen B. G., 2009, *The Evolving ISM in the Milky Way and Nearby Galaxies*,
Espaillat C., et al., 2014, *arXiv*, arXiv:1402.7103
Fedele D., van den Ancker M. E., Henning T., Jayawardhana R., Oliveira J. M., 2010, *A&A*, 510, A72
Flaherty K. M., Muzerolle J., 2008, *AJ*, 135, 966
Fuente A., Martín-Pintado J., Bachiller R., Rodríguez-Franco A., Palla F., 2002, *A&A*, 387, 977
Furlan E. et al., 2006, *ApJS*, 165, 568
Furlan E., et al., 2011, *ApJS*, 195, 3
Gammie C. F., 1996, *ApJ*, 457, 355
Gáspár A., Rieke G. H., Su K. Y. L., Balog Z., Trilling D., Muzerolle J., Apai D., Kelly B. C., 2009, *ApJ*, 697, 1578
Gutermuth R. A., Megeath S. T., Myers P. C., Allen L. E., Pipher J. L., Fazio G. G., 2009, *ApJS*, 184, 18
Haisch K. E., Jr., Lada E. A., Lada C. J., 2001a, *ApJL*, 553, L153
Haisch K. E., Jr., Lada E. A., Lada C. J., 2001, *AJ*, 121, 2065
Herbig G. H., 1960, *ApJS*, 4, 337
Hernández J., Calvet N., Briceño C., Hartmann L., Berlind P., 2004, *AJ*, 127, 1682
Hernández J., Calvet N., Hartmann L., Briceño C., Sicilia-Aguilar A., Berlind P., 2005, *AJ*, 129, 856
Hernández J. et al., 2007a, *ApJ*, 662, 1067
Hernández J. et al., 2007b, *ApJ*, 671, 1784
Hernández J., Hartmann L., Calvet N., Jeffries R. D., Gutermuth R., Muzerolle J., Stauffer J., 2008, *ApJ*, 686, 1195
Hernández J., Calvet N., Hartmann L., Muzerolle J., Gutermuth R., Stauffer J., 2009, *ApJ*, 707, 705
Hillenbrand L. A., 1997, *AJ*, 113, 1733
Hillenbrand L. A., White R. J., 2004, *ApJ*, 604, 741
Hillenbrand L. A., 2008, in Livio, M., Sahu K., Valenti J., eds, *Proc. STScI Symp. 19, A Decade of Extrasolar Planets around Normal Stars*. Space Telescope Science Institute, Baltimore, MD, p. 84
Hollenbach D. J., Yorke H. W., Johnstone D., 2000, in Mannings V., Boss A., Russell, S. S., eds, *Protostars and Planets IV*. Univ. Arizona Press, Tucson, AZ, p. 401
Houk, N., 1978, *Michigan catalogue of two-dimensional spectral types for the HD stars*. Dept. of Astronomy, University of Michigan, Ann Arbor. Distributed by University Microfilms International.
Hubickyj O., Bodenheimer P., Lissauer J. J., 2005, *Icarus*, 179, 415
Ida S., Lin D. N. C., 2004a, *ApJ*, 604, 388
Ida S., Lin D. N. C., 2004b, *ApJ*, 616, 567
Isobe T., Feigelson E. D., Nelson P. I., 1986, *ApJ*, 306, 490
Jeffries R. D., Naylor T., Walter F. M., Pozzo M. P., Devey C. R., 2009, *MNRAS*, 393, 538
Johansen A., Brauer F., Dullemond C., Klahr H., Henning T., 2008, *A&A*, 486, 597
Johnson J. A., Butler R. P., Marcy G. W., Fischer D. A., Vogt S. S., Wright J. T., Peek K. M. G., 2007, *ApJ*, 670, 833
Johnson J. A., Aller K. M., Howard A. W., Crepp J. R., 2010, *PASP*, 122, 905
Kennedy G. M., Kenyon S. J., 2008, *ApJ*, 673, 502
Kennedy G. M., Kenyon S. J., 2009, *ApJ*, 695, 1210
Kenyon S. J., Hartmann L., 1987, *ApJ*, 323, 714
Kenyon S. J., Hartmann L., 1995, *ApJS*, 101, 117
Kretke K. A., Lin D. N. C., Garaud P., Turner N. J., 2009, *ApJ*, 690, 407
Kroupa P. 2002, *Science* 295, 82
Lada E. A. 1999, in Lada C. J., Kylafis N. D., eds, *The Origin of Stars and Planetary Systems*. Kluwer, Dordrecht, p. 441

Table 1. Summary of target clusters.

	Cluster	Age ^a (Myr)	Distance ^b (pc)	References for the disk fraction study ^c
1	NGC 1333	1±1 (He08)	318 (LL03)	He08, Ma09, Ro11
2	Trapezium	1±1 (Mu02)	450 (LL03)	Ha01, He08, Ma09
3	ρ Oph	1±1 (Fe10)	125 (LL03)	Fe10
4	Taurus	1.5±1.5 (He08)	140 (El78)	Ha01, He08, Ke09, Ma09, Fe10, Ro11
5	Cha I	2±1 (Ro11)	170 (Lu08)	Ha01, He08, Ke09, Ma09, Fe10, Ro11
6	NGC 2068/71	2±1.5 (Ro11)	400 (LL03)	He08, Ma09, Ro11
7	IC 348	2.5±0.5 (He08)	320 (Ha01a)	Ha01, He08, Ke09, Ma09, Fe10, Ro11
8	σ Ori	3±1 (Ro11)	440 (He07a)	He08, Ma09, Fe10, Ro11
9	NGC 2264	3±1 (He08)	760 (Da08a)	Ha01, He08, Ma09
10	Tr 37	4±1 (He08)	900 (Si05)	He08, Ke09, Ma09, Ro11
11	Ori OB1bc	4±3 (He05)	443 (He05)	He05, He08, Ke09, Ma09, Ga09
12	Upper Sco	5±1 (Pr02)	144 (He05)	He05, He08, Ke09, Ma09, Ga09, Fe10, Ro11
13	NGC 2362	5±1 (He08)	1500 (Da08b)	Ha01, He08, Ke09, Ma09, Fe10, Ro11
14	γ Vel	5±1.5 (He08)	350 (He08)	He08, Ma09, Ro11
15	λ Ori	5±1 (He08)	450 (He09)	He08, Ma09
16	Per OB2	6±2 (He05)	320 (He05)	He05
17	η Cham	7±1 (He08)	100 (Ma99)	He08, Ma09, Ga09, Fe10, Ro11
18	Ori OB1a	8.5±1.5 (Br05)	330 (He05)	He05, He08, Ke09, Ma09, Ga09
19	NGC 7160	11±1 (He08)	900 (Si05)	He08, Ke09, Ma09, Ro11

Notes:

^aAdopted age with reference in parenthesis. ^bDistance with reference in parenthesis. ^cLiteratures for disk fraction study in the past. Note that some references show different cluster names (e.g., 25 Ori, which is named as Ori OB1a in our list).

References: Br05: Briceño et al. (2005); Da08a: Dahm (2008a); Da08b: Dahm (2008b); El78: Elias (1978); Fe10: Fedele et al. (2010); Ga09: Gáspár et al. (2009); Ha01a: Haisch et al. (2001a); Ha01b: Haisch et al. (2001b); He05: Hernández et al. (2005); He07a: Hernández et al. (2007a); He08: Hernández et al. (2008); He09: Hernández et al. (2009); Ke09: Kennedy & Kenyon (2009); LL03: Lada & Lada (2003); Lu08: Luhman (2008); Ma09: Mamajek (2009); Ma99: Mamajek et al. (1999); Mu02: Muench et al. (2002); Pr02: Preibisch et al. (2002); Ro11: Roccatagliata et al. (2011); Si05: Sicilia-Aguilar et al. (2005).

Table 2. Adopted spectral type for the boundary masses of intermediate-mass stars.

t^a (Myr)	SpType ^b		Boundary mass with Δt^c	
	$7 M_\odot$	$1.5 M_\odot$	$7 M_\odot$ ($\Delta t = \pm 2$ Myr)	$1.5 M_\odot$ ($\Delta t = \pm 2$ Myr)
1	B2.5	K5 (1.5–1.6 M_\odot)	$\gtrsim 7 M_\odot$	1.2–1.5 M_\odot
1.5	B3	K5 (1.2–1.5)	$\gtrsim 7 M_\odot$	1.2–<2.2 M_\odot
2	B3	K5 (1.2–1.5)	7	1.2–<2.2 M_\odot
2.5	B3	K5 (1.2–1.5)	6–7	1.2–1.8 M_\odot
3	B3	K4 (1.5–1.6)	> 6–7	1.2–1.6 M_\odot
4	B3	K4	7	1.4–1.8 M_\odot
5	B3	K4 (1.4–1.5)	7	>1.4–1.6 M_\odot
6	B3	K3	7	1.4–1.6 M_\odot
7	B3	K2	7	1.4–1.7 M_\odot
8.5	B3	K1	7	1.4–1.7 M_\odot
10	B2	K2	~ 7	1.3–1.5 M_\odot
11	B3	G7	7	>1.3–<1.7 M_\odot

Notes:

^aAge of cluster.

^bSpectral type for the boundary mass (7 and 1.5 M_\odot) based on the isochrone model by Siess et al. (2000). The range of stellar mass corresponding to the spectral type is shown in the parentheses when the range covers more than $\Delta M \geq 0.1 M_\odot$.

^cThe possible shift of boundary mass for the age spread of ± 2 Myr based on the isochrone model by Siess et al. (2000).

Lada, C. J., Adams, F. C., 1992, ApJ, 393, 278
 Lada, C. J., Lada, E. A., 2003, ARA&A, 41, 57
 Lada, C. J., Alves, J., Lada, E. A., 1996, AJ, 111, 1964
 Lada C. J. et al., 2006, AJ, 131, 1574
 Laughlin G., Bodenheimer P., Adams F. C., 2004, ApJL, 612, L73
 Lavalley M., Isobe T., Feigelson E., 1992, in Worrall D.

M., Biemesderfer C., Barnes J., eds, ASP Conf. Ser. Vol. 25, Astronomical Data Analysis Software and Systems I. Astron. Soc. Pac., San Francisco, p. 245
 Lin D. N. C., Bodenheimer P., Richardson D. C., 1996, Nature, 380, 606
 Lissauer J. J., Stevenson D. J., 2007, in Reipurth, B., Jewitt, D., Keil, K., eds., Protostars and Planets V. Univ.

Table 3. Intermediate-mass star selection and *JHK*/MIR IMDF of target clusters.

Cluster	Membership Ref ^a	Age (Myr)	SpT ^b	SpT Ref ^c	<i>JHK</i> IMDF ^d (%)	MIR Ref ^e	MIR IMDF ^f (%)
NGC 1333	St76,As97,Wi04	1±1	B2.5–K5	Win10,Co10,SB	17±17 (1/6)	Gu09	100±50 (4/4)
Trapezium	Hi97	1±1	B2.5–K5	Hi97	9±3 (8/89)	—	— ^g
ρ Oph	Wi08	1±1	B2.5–K5	Wi08	0±5 (0/20)	Wi08	80±20 (4/5)
Taurus	Fu06, Fu11	1.5±1.5	B3–K5	Fu06, Fu11	31±10 (9/29)	Fu06,Lu06	72±16 (21/29)
Cha I	Lu04	2±1	B3–K5	Lu04	29±13 (5/17)	Lu08	60±35 (3/5)
NGC 2068/71	Fl08	2±1.5	B3–K5	Fl08	15±11 (2/13)	Fl08	69±23 (9/13)
IC 348	Lu03	2.5±0.5	B3–K5	Lu03	0±3 (0/34)	La06	21±8 (7/34)
σ Ori	He07a	3±1	B3–K4	Ca10,Re09,SB	0±4 (0/23)	He07a	17±9 (4/23)
NGC 2264	Re02	3±1	B3–K4	Re02	0±2 (0/55)	—	— ^g
Tr 37	Si05	4±1	B3–K4	Si05,SB	3±2 (2/69)	Si05, Si06	22±10 (5/23)
Ori OB1bc	He05	4±3	B3–K4†	He05	4±2 (4/94)	—	— ^g
Upper Sco	Ca06	5±1	B3–K4	Ca06	0±1 (0/94)	Ca06	2±2 (2/94) ^h
NGC 2362	Da07	5±1	B3–K4	Da07	0±5 (0/19)	Da07	0±5 (0/19)
γ Vel	He08	5±1.5	B3–K4†	Ho78,SB	0±6 (0/17)	He08	0±6 (0/17)
λ Ori	He09	5±1	B3–K4†	He09	8±8 (1/13)	He09	4±4 (1/27)
Per OB2	He05	6±2	B3–K3†	He05	0±3 (0/31)	—	— ^g
η Cham	Me05	7±1	B3–K2	Me05	0±33 (0/3)	Me05	— ⁱ
Ori OB1a	He05	8.5±1.5	B2–K1†	He05	2±1 (2/98)	—	— ^g
NGC 7160	Si05	11±1	B3–G7	Si05	0±1 (0/82)	Si06	3±2 (2/78)

Notes:

^aReferences from which the members of the clusters were picked up. The IM stars that were used for deriving the *JHK* IMDF were obtained from these references. For the Trapezium Cluster, members are selected from Hi97, but only those whose stated membership probability is more than 50 % were used.

^bThe range of spectral type for the target mass range (1.57 M_{\odot}) for the cluster age listed in the third column. † shows cluster for which the observed spectral types of cluster members do not completely reach to the boundary spectral type for the lowest mass (see the main text).

^cReferences from which the spectral types in the clusters were obtained. For some clusters for which the spectral type listing in the published papers is incomplete, we supplemented the spectral type information with those listed in the SIMBAD database at <http://simbad.u-strasbg.fr/simbad/> (denoted as SB).

^dDerived *JHK* IMDF and uncertainties based on Poisson errors. Numbers in parentheses show the number of disk-harbours members over total number of members. For the treatment of Poisson errors for zero detection, see the main text.

^eReferences for the MIR photometric data.

^fDerived MIR IMDF and uncertainties based on Poisson errors. Numbers in the parentheses shows the number of disk harbouring members over total number of members). For the treatment of Poisson errors for zero disk harbouring members, see the main text.

^gThe clusters for which *Spitzer* MIR data are unavailable.

^hFor MIR disk classification of this cluster, we use the slope between [4.5] and [8] rather than [3.6] and [8] because Carpenter et al. (2006) does not list photometry data in [3.6]. However, Kennedy and Kenyon (2009) confirms that use of [4.5] instead of [3.6] does not change the classification.

ⁱMIR IMDF was not derived because of the small number of sample IM stars (<3).

References:

As97: Aspin & Sandell (1997); Ca06: Carpenter et al. (2006); Ca10: Caballero et al. (2010); Co10: Connelley & Greene (2010); Da07: Dahm & Hillenbrand (2007); Fl08: Flaherty & Muzerolle (2008); Fu06: Furlan et al. (2006); Gu09: Gutermuth et al. (2009) He05: Hernández et al. (2005); He07a: Hernández et al. (2007a); He08: Hernández et al. (2008); He09: Hernández et al. (2009); Hi97: Hillenbrand (1997); Ho78: Houk (1978); La06: Lada et al. (2006); Lu03: Luhman et al. (2003); Lu04: Luhman (2004); Lu06: Luhman et al. (2006); Lu08: Luhman et al. (2008); Me05: Megeath et al. (2005). Re02: Rebull et al. (2002); Re09: Renson & Manfroid (2009); Si05: Sicilia-Aguilar et al. (2005); Si06: Sicilia-Aguilar et al. (2006); St76: Strom et al. (1976); Wi04: Wilking et al. (2004); Wi08: Wilking, Gagné, & Allen (2008); Win10: Winston et al. (2010).

Table 4. Summary of disk lifetime.

	$< M_* >^a$	t_{JHK}^{life} (Myr)			t_{MIR}^{life} (Myr)		
		Yasui et al. (2010)	Survival	Binning ^b	Yasui et al. (2010)	Survival	Binning ^b
Intermediate-mass	2.5 M_{\odot}	—	2.8±2.4	3.3±0.9	—	6.1±4.2	6.7±1.1
Low-mass	0.5 M_{\odot}	9.7±1.1	—	—	8.6±0.7	—	—
Mass dependence			$M_*^{-0.8\pm0.7}$	$M_*^{-0.7\pm0.3}$		$M_*^{-0.2\pm0.3}$	$M_*^{-0.2\pm0.1}$

Notes:

^aCharacteristic mass for the mass range (see details in the main text).

^bSee Section 8.1 for the definition of this fitting.

- Arizona Press, Tucson, AZ, p. 591
- Liu M. C., Najita J., Tokunaga A. T., 2003, *ApJ*, 585, 372
- Luhman K. L., 2001, *ApJ*, 560, 287
- Luhman K. L., 2004, *ApJ*, 602, 816
- Luhman K. L., Stauffer J. R., Muench A. A., Rieke G. H., Lada E. A., Bouvier J., Lada C. J., 2003, *ApJ*, 593, 1093
- Luhman K. L., Whitney B. A., Meade M. R., Babler B. L., Indebetouw R., Bracker S., Churchwell E. B., 2006, *ApJ*, 647, 1180
- Luhman K. L., 2008a, in Reipurth, B., ed., *Handbook of Star Forming Regions, Volume II*. Astron. Soc. Pac., San Francisco, p. 169
- Luhman K. L. et al., 2008b, *ApJ*, 675, 1375
- Mamajek E. E., 2009, in Usuda T., Ishii M., Tamura, M., eds, *AIP Conf. Proc. Vol. 1158, Exoplanets and Disks: Their Formation and Diversity*. American Institute of Physics, Melville, NY, p. 3
- Mamajek E. E., Lawson W. A., Feigelson E. D., 1999, *ApJL*, 516, L77
- Mann R. K., Williams J. P., 2009, *ApJL*, 694, L36
- Mathews G. S., Williams J. P., Ménard F., Phillips N., Duchêne G., Pinte C., 2012, *ApJ*, 745, 23
- Meeus G., Waters L. B. F. M., Bouwman J., van den Ancker M. E., Waelkens C., Malfait K., 2001, *A&A*, 365, 476
- Meeus G., et al., 2012, *A&A*, 544, A78
- Megeath S. T., Hartmann L., Luhman K. L., Fazio G. G., 2005, *ApJL*, 634, L113
- Megeath S. T., Townsley L. K., Oey M. S., Tiefertunk A. R., 2008, *hsf1.book*, 264
- Mendigutía I., Calvet N., Montesinos B., Mora A., Muzerolle J., Eiroa C., Oudmaijer R. D., Mern B., 2011, *A&A*, 535, A99
- Millan-Gabet R., Malbet F., Akeson R., Leinert C., Monnier J., Waters R., 2007, in Reipurth, B., Jewitt, D., Keil, K., eds., *Protostars and Planets V*. Univ. Arizona Press, Tucson, AZ, p. 539
- Muench A. A., Lada E. A., Lada C. J., Alves J., 2002, *ApJ*, 573, 366
- Muzerolle J., Allen L. E., Megeath S. T., Hernández J., Gutermuth R. A., 2010, *ApJ*, 708, 1107
- Nakagawa Y., Nakazawa K., Hayashi C., 1981, *Icarus*, 45, 517
- Natta A., Prusti T., Neri R., Wooden D., Grinin V. P., Mannings V., 2001, *A&A*, 371, 186
- Palla F., Stahler S. W., 2000, *ApJ*, 540, 255
- Papaloizou J. C. B., Nelson R. P., Kley W., Masset F. S., Artymowicz P., 2007, *Protostars and Planets V*, in Reipurth, B., Jewitt, D., Keil, K., eds., *Protostars and Planets V*. Univ. Arizona Press, p. 655
- Pinte C., et al., 2008, *A&A*, 489, 633
- Preibisch T., Brown A. G. A., Bridges T., Guenther E., Zinnecker H., 2002, *AJ*, 124, 404
- Rebull L. M. et al., 2002, *AJ*, 123, 1528
- Reipurth B., 2008, *hsf1.book*,
- Reipurth B., 2008, *hsf2.book*,
- Renson P., Manfroid J., 2009, *A&A*, 498, 961
- Robinson S. E., Laughlin G., Bodenheimer P., Fischer D., 2006, *ApJ*, 643, 484
- Roccatagliata V., Bouwman J., Henning T., Gennaro M., Feigelson E., Kim J. S., Sicilia-Aguilar A., Lawson W. A., 2011, *ApJ*, 733, 113
- Schaefer G. H., Simon M., Beck T. L., Nelan E., Prato L., 2006, *AJ*, 132, 2618
- Shu F. H., Adams F. C., Lizano S., 1987, *ARA&A*, 25, 23
- Sicilia-Aguilar A., Hartmann L. W., Briceño C., Muzerolle J., Calvet N., 2004, *AJ*, 128, 805
- Sicilia-Aguilar A., Hartmann L. W., Hernández J., Briceño C., Calvet N., 2005, *AJ*, 130, 188
- Sicilia-Aguilar, A., et al., 2006, *ApJ*, 638, 897
- Siess L., Dufour E., Forestini M., 2000, *A&A*, 358, 593
- Simon M., Dutrey A., Guilloteau S., 2000, *ApJ*, 545, 1034
- Strom K. M., Strom S. E., Edwards S., Cabrit S., Skrutskie M. F., 1989, *AJ*, 97, 1451
- Tanaka H., Himeno Y., Ida S., 2005, *ApJ*, 625, 414
- Strom S. E., Vrba F. J., Strom K. M., 1976, *AJ*, 81, 314
- Tognelli E., Prada Moroni P. G., Degl’Innocenti S., 2011, *A&A*, 533, A109
- Trilling D. E., Lunine J. I., Benz W., 2002, *A&A*, 394, 241
- Trilling D. E., Benz W., Guillot, T., Lunine J. I., Hubbard W. B., Burrows A., 1998, *ApJ*, 500, 428
- Uzpen B., Kobulnicky H. A., Kinemuchi K., 2009, *AJ*, 137, 3329
- Villaver E., Livio M., 2009, *ApJL*, 705, L81
- Weidenschilling S. J., 1997, *Icarus*, 127, 290
- Wilking B. A., Meyer M. R., Greene T. P., Mikhail A., Carlson G., 2004, *AJ*, 127, 1131
- Wilking B. A., Gagné M., Allen L. E., 2008, in Reipurth, B., ed., *Handbook of Star Forming Regions, Volume II*. Astron. Soc. Pac., San Francisco, p.351
- Williams J. P., Cieza L. A., 2011, *ARA&A*, 49, 67
- Winston E., et al., 2010, *AJ*, 140, 266
- Wolff S. C., Strom S. E., Rebull L. M., 2011, *ApJ*, 726, 19
- Wolk S. J., Walter F. M., 1996, *AJ*, 111, 2066
- Wright, J. T., Upadhyay, S., Marcy, G. W., Fischer D. A., Ford E. B., Johnson J. A., 2009, *ApJ*, 693, 1084
- Wyatt M. C., Clarke C. J., Greaves J. S., 2007, *MNRAS*, 380, 1737
- Yasui C., Kobayashi N., Tokunaga A. T., Saito, M., Tokoku, C., 2009, *ApJ*, 705, 54
- Yasui C., Kobayashi N., Tokunaga A. T., Saito M., Tokoku C., 2010, *ApJL*, 723, L113
- Yi S. K., Kim Y.-C., Demarque P., 2003, *ApJS*, 144, 259
- Zinnecker H., Yorke H. W., 2007, *ARA&A*, 45, 481

APPENDIX A: LIST OF SAMPLE INTERMEDIATE-MASS STARS IN TARGET CLUSTERS

In this appendix, the intermediate-mass star samples for all 19 clusters listed in Table 3 are summarized in tables (Tabs. A1–A19) as well as in colour–colour diagrams (Figs. A1–A19).

In the tables, only RA, Dec coordinates (in J2000) are shown in case objects names are not available in the references. “SpT” shows the spectral types in the literatures. The “K disk” and “MIR disk” columns show objects with a disk (o) and without a disk (X). The numbers in the parenthesis in MIR disk column is α as defined in Section 1. The stars with K-disk emission are judged from the colour–colour diagram, in which the red and black circles show those with a K disk and without a K disk, respectively.

Table A1. NGC 1333.

The α values for MIR disk are directly referred from Gutermuth et al. (2009). Though extinction is not corrected for α values in this reference, it should not affect the disk judgement because the α value is much larger than -2 . The spectral type with * mark is from SIMBAD database.

Name	RAJ2000 (h:m:s)	DEJ2000 (d:m:s)	SpT	<i>K</i> disk	MIR disk
2MASS J03291977+3124572	03 29 19.77605	+31 24 57.0474	B8*	X	...
2MASS J03285720+3114189	03 28 57.2107	+31 14 19.056	B*	X	...
2MASS J03290575+3116396	03 29 05.754	+31 16 39.69	A3	X	o (−0.28)
2MASS J03291037+3121591 (LZK 12)	03 29 10.379	+31 21 59.16	F4–G0	o	o (−0.40)
2MASS J03285930+3115485	03 28 59.306	+31 15 48.52	K2	X	o (−0.25)
2MASS J03292187+3115363 (LkHA 271)	03 29 21.873	+31 15 36.30	K4.0	X	o (−1.49)

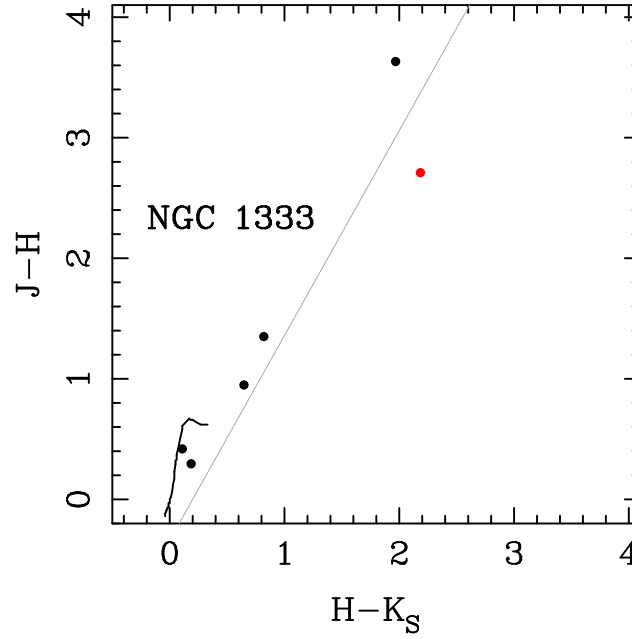


Figure A1. NGC1333.

Table A2. Trapezium.

RAJ2000 (h:m:s)	DEJ2000 (d:m:s)	SpT	<i>K</i> disk
05 35 06.08	−05 12 15.22	B3–B5	X
05 35 31.35	−05 25 15.92	B3–B6	X
05 35 40.06	−05 17 29.12	B6	X
05 35 54.10	−05 37 42.50	B5–B7	X
05 34 39.93	−05 10 06.81	B8–A0	X
05 34 55.20	−05 30 21.52	B8–B9	X
05 35 00.03	−05 25 15.82	B9–A1	X
05 35 58.45	−05 22 30.62	B8–B9.5	X
05 35 28.32	−05 26 19.82	B9.5–A0V	X
05 35 16.88	−05 21 45.02	A0–A2	X
05 34 46.90	−05 34 14.82	B9–A1	X
05 36 27.08	−05 24 30.20	B9–A0	X
05 35 55.33	−05 13 55.52	A0–A5	X
05 35 35.67	−05 12 20.32	B9–A1	X
05 34 49.91	−05 18 44.42	A2–A7	o
05 35 50.36	−05 28 34.62	B8–A5	o
05 35 19.03	−05 20 38.52	B5–A7	X
05 35 18.70	−05 17 28.92	A8–F0	o
05 35 15.89	−05 23 52.52	F2–F7	X
05 35 31.28	−05 33 08.62	A8–F8	o
05 35 54.65	−05 10 55.22	F7–G4	X
05 35 05.11	−05 14 50.22	F8–G5	X
05 35 18.57	−05 20 33.52	F8–K0	X
05 35 11.53	−05 16 57.52	G0–K0	X
05 34 24.83	−05 22 05.09	G0–G1	X
05 35 21.16	−05 09 15.82	F8–K2	o
05 35 26.75	−05 11 07.12	G3	o
05 34 19.39	−05 27 11.57	G6	X
05 34 14.39	−05 28 16.30	G6–K0	X
05 35 26.10	−05 27 36.22	G3–K3	X
05 35 15.15	−05 22 56.42	G6–G8	...
05 35 35.89	−05 12 25.02	G6–K2	o
05 35 21.70	−05 23 53.62	G6–K3	X
05 35 20.94	−05 23 48.62	G8–K5	X

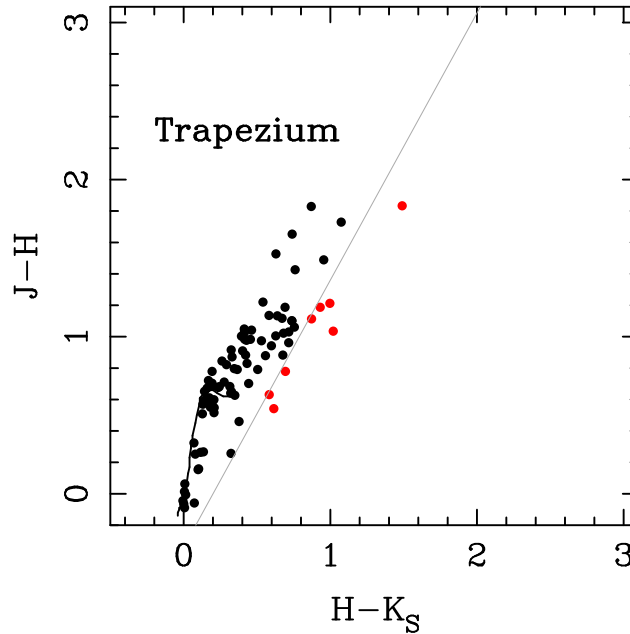
**Figure A2.** Trapezium.

Table A2 – *continued*

RAJ2000 (h:m:s)	DEJ2000 (d:m:s)	SpT	<i>K</i> disk
05 35 26.19	−05 08 39.72	G8–K5.5	...
05 35 15.53	−05 22 56.12	G8–K1	X
05 35 18.95	−05 23 49.22	G8–K5	...
05 35 21.21	−05 12 12.42	G8–G0	X
05 35 28.49	−05 31 26.12	G	X
05 35 02.75	−05 22 07.92	G	X
05 34 53.52	−05 26 36.72	G	X
05 35 20.11	−05 20 56.72	F7–K3	o
05 35 05.55	−05 25 19.02	A0–K4	X
05 35 23.73	−05 30 46.92	G8–K3	X
05 35 41.87	−05 28 12.42	K0–K1	X
05 35 54.56	−05 22 00.72	K0–K2	X
05 35 16.96	−05 23 33.72	K0–K2	...
05 35 11.77	−05 19 26.02	K0–K3	...
05 35 14.60	−05 39 11.42	K0–K3	X
05 35 20.65	−05 15 49.12	K0–K5	X
05 35 15.85	−05 23 49.42	G5–K0	X
05 35 25.63	−05 09 49.22	K0–K4	X
05 34 39.80	−05 26 41.62	K0–K3	X
05 35 21.18	−05 24 56.92	K1–K2	X
05 35 02.91	−05 30 00.92	K1–K2	X
05 35 34.81	−05 29 14.02	K1–K4	X
05 35 35.05	−05 33 49.02	K1–K5	X
05 35 31.18	−05 15 32.92	K1	X
05 35 38.74	−05 12 41.72	K2	X
05 35 08.29	−05 28 28.92	K2	X
05 34 51.48	−05 25 12.62	K2	X
05 35 19.19	−05 20 07.72	K2	X
05 34 33.87	−05 28 24.22	K2	X
05 34 45.10	−05 25 03.62	K2	X
05 34 55.89	−05 23 12.62	K0–K4	X
05 35 53.53	−05 15 41.42	K2–K3	X
05 35 17.41	−05 17 39.82	K2–K3	X
05 35 11.40	−05 26 01.82	K2–K3	X
05 35 13.69	−05 39 10.52	K2–K4	X
05 35 24.98	−05 23 46.32	K2–K4	X
05 35 15.96	−05 20 36.32	K2–K4	X
05 35 18.55	−05 23 13.52	K2–K5	...
05 34 37.35	−05 34 51.92	K2–K5	X
05 34 35.05	−05 32 10.22	K2	X
05 35 25.30	−05 10 47.92	K3	X
05 35 02.30	−05 15 47.82	K3	X
05 36 10.38	−05 19 44.62	K1–K3	X
05 35 29.74	−05 32 53.12	G8–K3	X
05 35 22.15	−05 20 29.02	K2–K4	X
05 35 17.50	−05 22 56.22	K3–K4	X
05 35 18.79	−05 16 13.72	K2–K5	X
05 35 14.88	−05 21 59.62	K3–K4	X
05 35 31.13	−05 23 39.72	K3–K5	X
05 35 05.52	−05 11 50.62	K3–K5	X
05 35 35.17	−05 21 26.92	K4	...
05 35 08.75	−05 31 48.52	K4	X
05 35 27.19	−05 23 36.32	K4	X
05 35 26.31	−05 23 01.92	K4–K5	...
05 35 04.43	−05 29 37.82	K4–K5	...
05 35 24.14	−05 25 18.32	K0–K5	X
05 35 50.66	−05 16 29.02	K5	X
05 35 23.54	−05 23 31.62	K5	...
05 35 21.47	−05 09 38.72	K5	X
05 35 20.90	−05 31 21.22	K5	X
05 35 06.19	−05 22 02.32	K5	X
05 35 04.67	−05 17 42.12	K5	X
05 35 02.34	−05 20 46.32	K5	X
05 34 58.71	−05 21 17.52	K5	X
05 34 50.63	−05 24 01.02	K5	...

Table A3. ρ Oph.

Because we could not find published IRAC photometry data, we directly used the MIR disk classification in Wilking, Gagné, & Allen (2008).

RAJ2000 (h:m:s)	DEJ2000 (d:m:s)	SpT	K disk	MIR disk
16 26 9.31	−24 34 12.10	A0 V	X	...
16 27 49.87	−24 25 40.20	A7	X	X
16 28 25.16	−24 45 0.90	F2 V	X	...
16 25 7.93	−24 31 57.20	F5	X	...
16 27 10.28	−24 19 12.70	G1	X	o
16 25 19.24	−24 26 52.60	G1IV	X	...
16 26 46.43	−24 12 0.10	G3.5	X	...
16 26 23.36	−24 20 59.80	G6	X	o
16 28 32.66	−24 22 44.90	G7	X	...
16 26 3.02	−24 23 36.00	K0	X	...
16 26 58.51	−24 45 36.90	K1
16 27 17.08	−24 47 11.20	K1	X	...
16 25 24.35	−23 55 10.30	K3/M0: (BA92)	X	...
16 25 49.64	−24 51 31.90	K3/M0 (BA92W94)	X	...
16 24 56.52	−24 59 38.20	K5	X	...
16 25 22.43	−24 02 5.70	K5	X	...
16 26 23.68	−24 43 13.90	K5	X	...
16 27 39.43	−24 39 15.50	K5	X	o
16 27 40.29	−24 22 4.00	K5	X	o
16 28 16.73	−24 05 14.30	K5	X	...
16 28 23.33	−24 22 40.60	K5	X	...

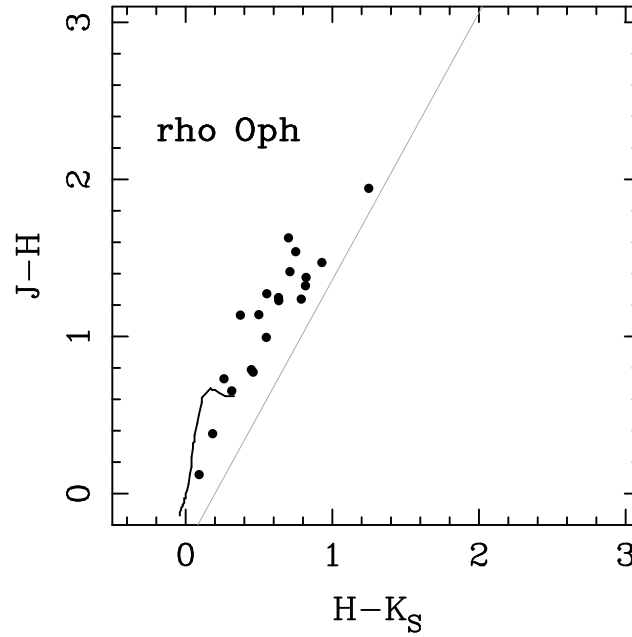
**Figure A3.** ρ Oph.

Table A4. Taurus.

The † and ‡ marks show the members that are identified as w/disks or w/o disks from SEDs in Furlan et al. (2006) and Furlan et al. (2011), respectively.

Name	SpT	K disk	MIR disk
V892 Tau	B9	o	o†
AB Aur	A0	o	o†
HP Tau/G2	G0	X	X†
RY Tau	G1	X	o†
SU Aur	G1	X	o†
HD 283572	G5	X	X (−2.82)
IRAS 04278+2253	G8	X	o‡
LkCa 19	K0	X	X‡
T Tau	K0	o	o†
HBC 388	K1	X	X†
HQ Tau	K2	X	o†
IT Tau	K2	X	o (−1.47)
CW Tau	K3	o	o†
HP Tau	K3	o	o†
RW Aur	K3	X	o†
V773 Tau	K3	X	o†
HBC 356	K3	X	X†
V410 Tau	K3	X	X (−2.79)
2MASS J04390525+2337450	K5	X	o‡
DR Tau	K5	o	o†
DS Tau	K5	o	o†
FV Tau (A, B)	K5	X	o (−0.90)
FS Tau B (Haro 6-5B)	K5	o	o‡
HN Tau (A, B)	K5	o	o†
LkCa 15	K5	X	o †
UX Tau (A, Ba, Bb, C)	K5	X	o†
V807 Tau	K5	X	o†
HBC 392	K5	X	X†
HBC 427	K5	X	X†

Notes:

The sample includes two low-mass stars with measured dynamical masses, Lk Ca 15 (Hillenbrand & White 2004; $0.84 M_{\odot}$) and V807 Tau (Schaefer et al. 2006; $1.15 M_{\odot}$). By our criteria, both objects have spectral type of K5 and are classified as IM stars. The dynamical mass of V807 Tau is almost within the mass uncertainty of our method as described in section 2.2. Lk Ca 15 has an estimated age (3–5 Myr; Simon, Dutrey, & Guilloteau 2000) that is much higher than the average Taurus cluster age (1.5 Myr; see also Fig. 3 in Simon et al. 2000), which we employed for our IM star selection (see § 2.2 and § 8.1.2). However, these stars are included for consistency with the other clusters. As discussed in section 2.2 up to 15 % of our sample of IM stars could be low mass stars.

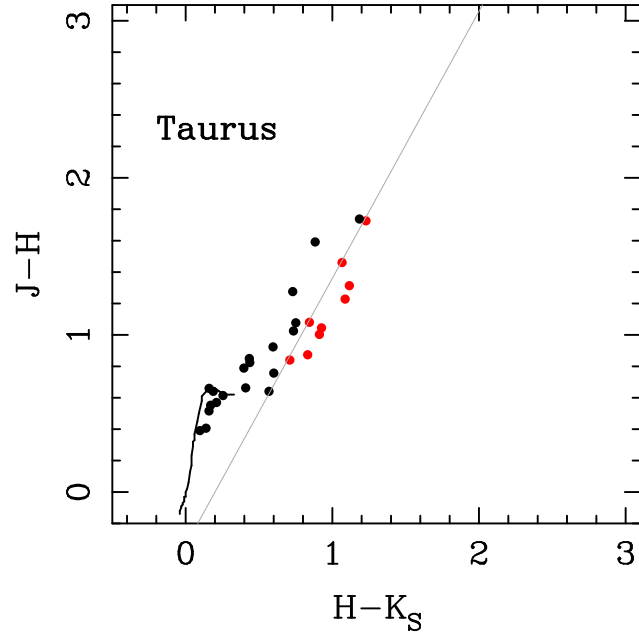


Figure A4. Taurus.

Table A5. Cha I.

RAJ2000 (h:m:s)	DEJ2000 (d:m:s)	SpT	K disk	MIR disk
11 05 57.81	−76 07 48.9	B6.5	X	...
11 08 03.30	−77 39 17.4	B9.5	o	...
11 09 50.03	−76 36 47.7	B9	X	...
10 46 37.95	−77 36 03.6	F0	X	...
11 06 15.41	−77 21 56.8	G5	X	X (-2.67)
11 07 20.74	−77 38 07.3	G2	o	...
11 08 15.10	−77 33 53.2	G7	o	...
11 12 27.72	−76 44 22.3	G9	X	o (-1.27)
11 12 42.69	−77 22 23.1	G8	X	...
10 58 16.77	−77 17 17.1	K0	X	...
10 59 06.99	−77 01 40.4	K2	X	...
11 10 38.02	−77 32 39.9	K3	X	o (-1.24)
11 12 24.41	−76 37 06.4	K3.5	X	o (-0.57)
11 12 43.00	−76 37 04.9	K4.5	X	X (-2.78)
11 04 09.09	−76 27 19.4	K5	X	...
11 09 53.41	−76 34 25.5	K5	o	...
11 10 00.11	−76 34 57.9	K5	o	...

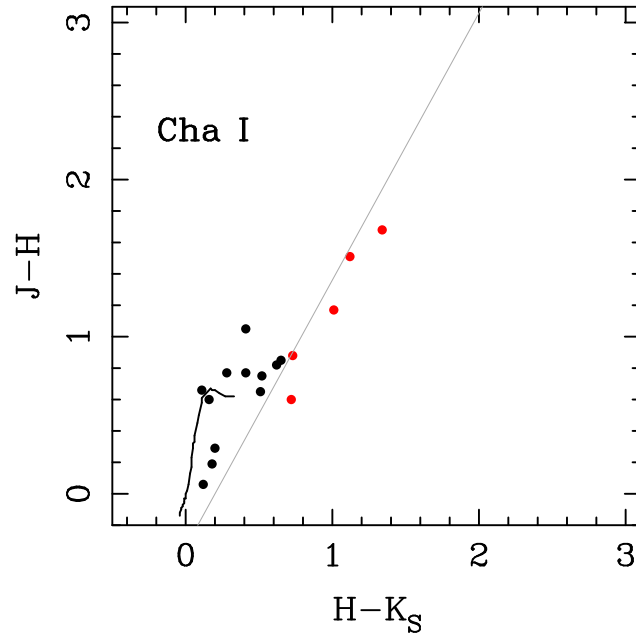


Figure A5. Cha I.

Table A6. NGC 2068/71.

Name (FM2008)	RAJ2000 (h:m:s)	DEJ2000 (d:m:s)	SpT	<i>K</i> disk	MIR disk
1173	05 47 10.98	+00 19 14.81	G6	X	o (−1.08)
1099	05 47 06.00	+00 32 08.48	K0	o	o (−1.04)
618	05 46 22.44	−00 08 52.62	K1	X	o (−1.64)
571	05 46 18.30	+00 06 57.85	K1	X	o (−0.73)
515	05 46 11.86	+00 32 25.91	K2	X	X (−2.24)
590	05 46 19.47	−00 05 20.00	K2.5	X	o (−0.65)
984	05 46 56.54	+00 20 52.91	K3	X	X (−2.46)
458	05 46 07.89	−00 11 56.87	K3	X	o (−1.92)
739	05 46 34.54	+00 06 43.45	K4	X	o (−1.12)
581	05 46 18.89	−00 05 38.11	K4	X	o (−1.27)
177	05 45 41.94	−00 12 05.33	K4	X	X (−2.63)
1116	05 47 06.96	+00 00 47.74	K4.5	X	o (−0.95)
584	05 46 19.06	+00 03 29.59	K5	o	o (−1.00)

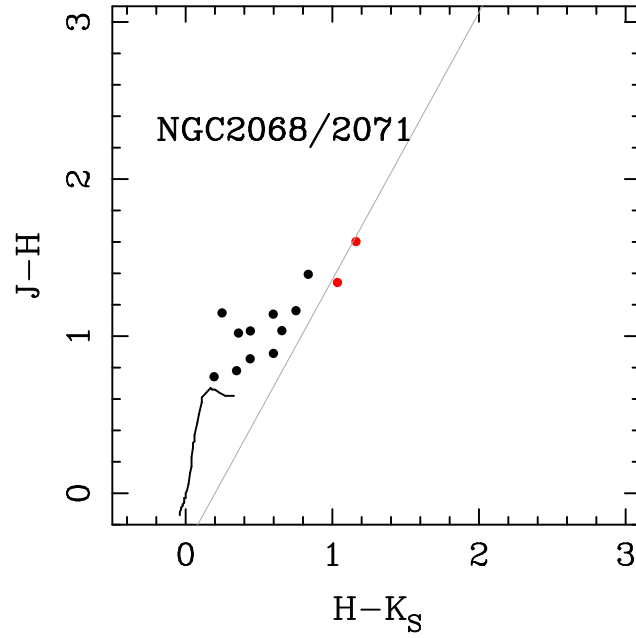
**Figure A6.** NGC 2068/71.

Table A7. IC 348.

RAJ2000 (h:m:s)	DEJ2000 (d:m:s)	SpT	K disk	MIR disk
03 44 34.20	+32 09 46.3	B5	X	X (−2.58)
03 44 08.48	+32 07 16.5	A0	X	X (−2.79)
03 44 50.65	+32 19 06.8	A0	X	X (−2.82)
03 44 30.82	+32 09 55.8	A2	X	o (−0.73)
03 44 09.15	+32 07 09.3	A2	X	X (−2.53)
03 44 35.36	+32 10 04.6	A2	X	o (−1.37)
03 44 32.06	+32 11 44.0	A3
03 45 01.42	+32 05 02.0	A4	X	X (−2.69)
03 44 47.72	+32 19 11.9	A4	X	X (−2.70)
03 44 19.13	+32 09 31.4	F0	X	X (−2.81)
03 44 31.19	+32 06 22.1	F0	X	X (−2.79)
03 44 24.66	+32 10 15.0	F2	X	X (−2.82)
03 44 23.99	+32 11 00.0	G0	X	X (−2.77)
03 44 31.96	+32 11 43.9	G0	X	o (1.01)
03 44 18.16	+32 04 57.0	G1	X	o (−1.66)
03 45 07.61	+32 10 28.1	G1	X	X (−2.67)
03 44 36.94	+32 06 45.4	G3	X	o (−1.93)
03 45 07.96	+32 04 02.1	G4	X	X (−2.68)
03 43 51.24	+32 13 09.4	G5	X	X (−2.70)
03 44 32.74	+32 08 37.5	G6	X	X (−2.75)
03 44 39.17	+32 09 18.3	G8	X	X (−2.89)
03 44 26.03	+32 04 30.4	G8	X	o (−1.31)
03 45 01.52	+32 10 51.5	K0	X	X (−2.60)
03 44 16.43	+32 09 55.2	K0	X	X (−2.77)
03 43 55.51	+32 09 32.5	K0	X	X (−2.61)
03 44 08.86	+32 16 10.7	K0	X	X (−2.72)
03 44 56.15	+32 09 15.5	K0	X	o (−1.88)
03 44 40.13	+32 11 34.3	K2	X	X (−2.66)
03 44 31.53	+32 08 45.0	K2	X	X (−2.70)
03 44 39.25	+32 07 35.5	K3	X	X (−2.60)
03 44 38.72	+32 08 42.0	K3	X	X (−2.91)
03 44 05.00	+32 09 53.8	K3.5	X	X (−2.77)
03 45 01.74	+32 14 27.9	K4	X	X (−2.75)
03 44 55.63	+32 09 20.2	K4	X	X (−2.74)
03 44 24.29	+32 10 19.4	K5	X	X (−2.68)

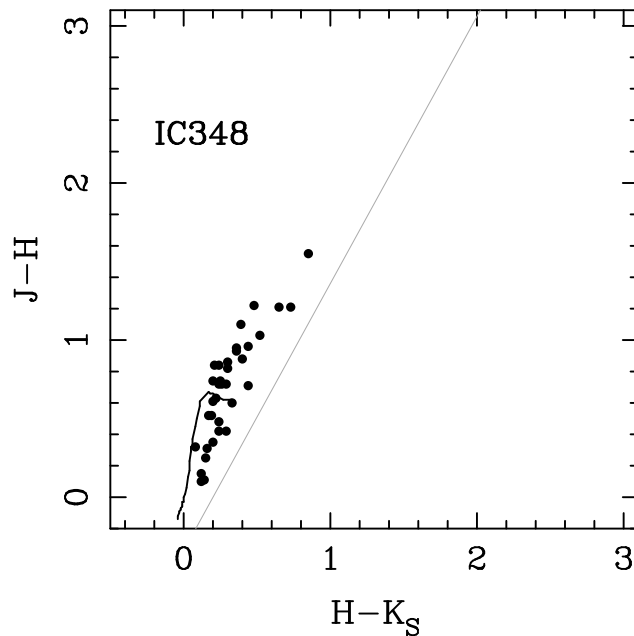

Figure A7. IC 348.

Table A8. σ Ori.

The spectral type with * mark is from SIMBAD database.

Name	RAJ2000 (h:m:s)	DEJ2000 (d:m:s)	SpT	<i>K</i> disk	MIR disk
HD 37525	05 39 01.49131	−02 38 56.3650	B5	X	X (−2.85)
HD 294271	05 38 36.5494	−02 33 12.740	B5V*	X	X (−2.91)
2MASS J05383422−0234160	05 38 34.235	−02 34 16.08	B8V*	X	X (−2.81)
HD 37545	05 39 09.2145	−02 56 34.732	B9*	X	X (−2.79)
V1147 Ori	05 39 46.1950	−02 40 32.054	B9	X	X (−2.81)
HD 294272	05 38 34.799	−02 34 15.78	B9.5III	X	X (−2.91)
HD 37564	05 39 15.0594	−02 31 37.618	A0*	X	X (−2.51)
HD 294275	05 37 31.8728	−02 45 18.473	A1V*	X	X (−2.81)
HD 294279	05 38 31.3795	−02 55 03.075	A2*	X	X (−2.76)
HD 294273	05 38 27.5241	−02 43 32.596	A3*	X	X (−2.87)
HD 294299	05 39 40.572	−02 25 46.82	F2*	X	X (−2.76)
HD 294268	05 38 14.1139	−02 15 59.741	F8*	X	o (0.17)
HD 294274	05 37 45.3662	−02 44 12.491	G0*	X	X (−2.85)
HD 294298	05 39 59.318	−02 22 54.35	G0*	X	X (−2.84)
2MASS J05375303−0233344	05 37 53.036	−02 33 34.41	K0	X	X (−2.82)
2MASS J05383848−0234550	05 38 38.486	−02 34 55.02	K0	X	X (−2.63)
2MASS J05393654−0242171	05 39 36.543	−02 42 17.16	K0*	X	X (−2.79)
2MASS J05375440−0239298	05 37 54.405	−02 39 29.85	K0:	X	X (−2.86)
TY Ori	05 38 35.873	−02 43 51.22	K3*	X	o (−1.85)
2MASS J05384129−0237225	05 38 41.292	−02 37 22.57	K3	X	X (−2.78)
2MASS J05384803−0227141	05 38 48.036	−02 27 14.19	K3	X	o (−1.55)
2MASS J05385410−0249297	05 38 54.107	−02 49 29.77	K3*	X	X (−2.80)
TX Ori	05 38 33.685	−02 44 14.15	K4*	X	o (−0.97)

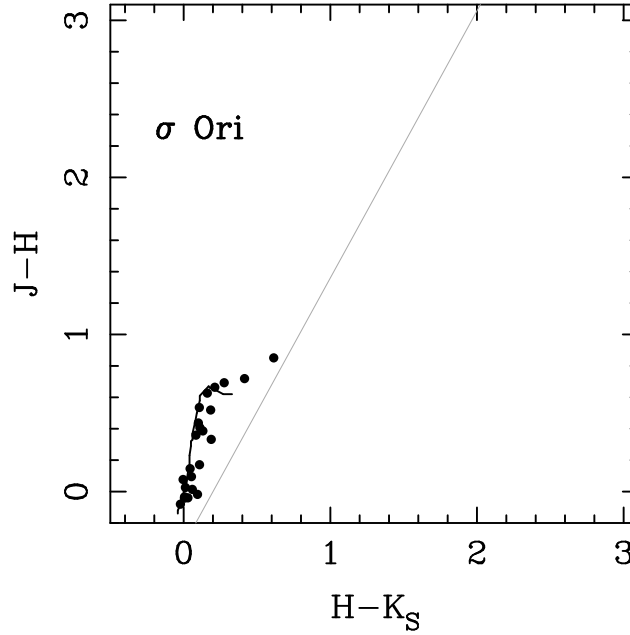
**Figure A8.** σ Ori.

Table A9. NGC 2264.

RAJ2000 (h:m:s)	DEJ2000 (d:m:s)	SpT	<i>K</i> disk
06 41 32.7	+09 53 24	A2	X
06 41 27.7	+09 55 13	A2	X
06 41 36.6	+09 37 56	A5	X
06 41 24.3	+09 46 10	A5	X
06 40 39.3	+09 59 22	A5	X
06 40 47.0	+09 55 03	F0	X
06 40 37.8	+09 40 11	F0	X
06 41 26.2	+09 47 22	F1	X
06 41 24.3	+09 56 09	F1	X
06 40 50.4	+09 54 16	F1	X
06 41 26.0	+09 57 15	F3	X
06 40 33.5	+09 42 55	F5	X
06 41 13.8	+09 55 44	G0	X
06 40 37.3	+09 42 15	G0	X
06 39 41.6	+09 34 40	G0	X
06 40 41.4	+09 54 13	G1	X
06 41 08.9	+09 46 01	G2.5	X
06 41 03.5	+09 31 19	G3	X
06 40 56.6	+09 54 10	G4	X
06 41 29.2	+09 39 36	G5	X
06 41 04.5	+09 51 50	G5	X
06 39 46.8	+09 40 54	G5	X
06 40 59.4	+09 55 20	G6	X
06 40 59.4	+09 55 20	G6	X
06 40 21.1	+09 36 32	G6	X
06 41 06.8	+09 34 46	G6:	X
06 40 09.7	+09 41 43	G9	X
06 41 02.6	+09 34 56	K0	X
06 41 02.3	+09 51 52	K0	X
06 39 43.6	+09 36 04	K0	X
06 41 23.3	+09 52 42	K0:	X
06 41 15.4	+09 46 40	K1	X
06 41 06.9	+09 23 22	K1.5	X
06 41 00.3	+09 58 49	K1.5	X
06 41 01.0	+09 32 45	K1:	X
06 41 36.8	+09 58 20	K2	X
06 41 31.6	+09 48 33	K2	X
06 41 27.2	+09 35 07	K2	X
06 41 05.0	+09 50 46	K2	X
06 40 58.8	+09 30 57	K2	X
06 40 48.8	+09 32 43	K2	X
06 40 47.6	+09 49 29	K2	X
06 40 45.2	+09 28 45	K2	X
06 40 30.0	+09 50 10	K2	X
06 41 04.2	+09 52 02	K3	X
06 41 00.5	+09 45 03	K3	X
06 41 21.5	+09 58 35	K4	X
06 41 18.3	+09 33 54	K4	X
06 41 16.8	+09 27 30	K4	X
06 41 09.4	+09 59 38	K4	X
06 41 01.6	+10 00 36	K4	X
06 40 51.6	+09 43 24	K4	X
06 40 39.2	+09 50 58	K4	X
06 40 30.7	+09 46 11	K4	X
06 40 28.8	+09 31 01	K4	X
06 40 16.1	+09 57 37	K4	X

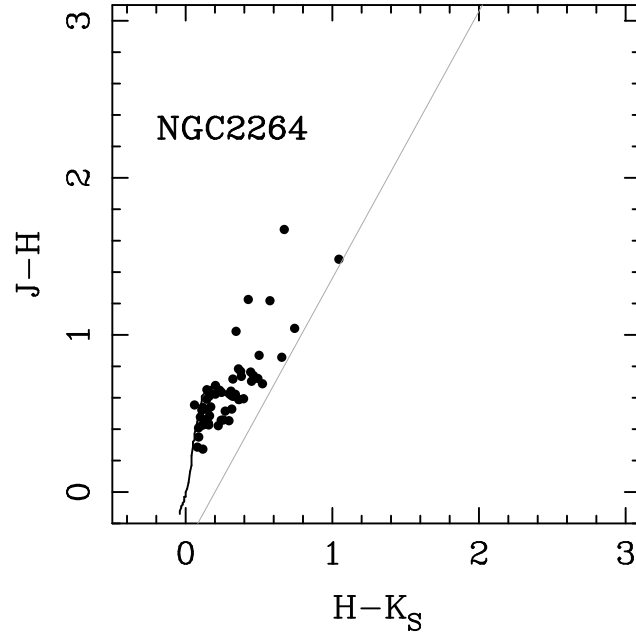


Figure A9. NGC 2264.

Table A10. Tr 37. The spectral type with * mark is from SIMBAD database.

Name	SpT	K disk	MIR disk
CCDM+5734Ae	B3	X	X (−2.61)
MVA-63	B4	X	...
MVA-1312	B4	X	...
CCDM+5734Aw	B5	X	X (−2.61)
MVA-805	B6	X	...
MVA-437	B7	X	X (−2.78)
AG+561491	B7	X	...
MVA-426	B7	o	...
MVA-468	B7	X	X (−2.32)
MVA-252	B7	X	...
MVA-182	B8	X	...
KUN-196	B9	X	o (−1.86)
MVA-662	B9	X	X (−2.60)
MVA-535	B9	X	X (−2.80)
MVA-463	A0	X	...
SBZ-2-46	A0	X	...
MVA-81	A0	X	...
tr37-185	A1	X	...
BD+572362	A1	X	...
MVA-497	A1	X	...
MVA-566	A1	X	...
KUN-318	A1	X	X (−2.90)
KUN-197	A2	X	X (−2.93)
MVA-660	A2	X	...
MVA-258	A2	X	...
MVA-164	A3	X	...
BD+572355	A4	X	X (−2.67)
MVA-169	A4	X	...
MVA-640	A7	X	...
BD+572356	A7	X	X (−2.74)
MVA-545	A7	X	...
MVA-224e	A7	X	X (−2.94)
KUN-89	A8	X	X (−2.66)
MVA-472	A8	X	...
MVA-564	A9	X	...
MVA-657	F0	X	...
KUN-87	F0	X	...
MVA-447	F0	X	...
KUN-93	F1	X	X (−2.79)
KUN-327	F1	X	...
KUN-100	F3	X	...
KUN-198	F3	X	X (−2.58)
KUN-191	F5	X	X (−2.83)
KUN-97	F6	X	...
KUN-58	F6	X	...
KUN-85	F7	X	...
MVA-523	F7	X	...
MVA-232	F7	X	X (−2.77)
KUN-92	F9	X	...
KUN-86	F9	X	o (−2.15)
KUN-84	F9	X	...
KUN-83	F9	X	X (−3.04)
MVA-234	F9	X	...
KUN-56	F9	X	...
KUN-314S	A*	o	...
KUN-56	F9.0	X	...
[SHB2004] 11-581	G	X	X (−2.79)
[SHB2004] 11-1864	G–K	...	X (−2.35)
[SHB2004] 93-361	G1
[SHB2004] 13-277	G1	X	o (−0.76)
[SHB2004] 73-537	G1.5	...	o (−0.88)
[SHB2004] 12-1091	G2.5	X	o (−1.17)

Table A10 – *continued*

Name	SpT	<i>K</i> disk	MIR disk
[SHB2004] 22-404	G7	X	...
[SHB2004] 21-1974	G7.5	X	...
[SHB2004] 82-272	G9	X	o (−1.20)
[SHB2004] 13-669	K1	X	o (−1.01)
[SHB2004] 13-236	K2	X	o (−1.35)
[SHB2004] 11-2031	K2	X	o (−0.75)
[SHB2004] 24-542	K4	X	X (−2.70)
[SHB2004] 13-1087	K4	X	X (−2.69)
[SHB2004] 12-94	K4	X	X (−2.55)

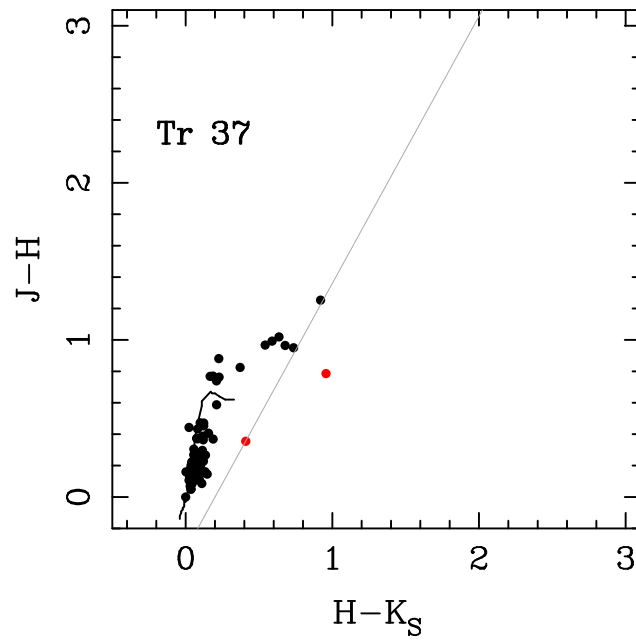


Figure A10. Tr 37.

Table A11. Ori OB1bc.

RAJ2000 (h:m:s)	DEJ2000 (d:m:s)	SpT	K disk
05 41 08.1	−03 37 57	B3	X
05 35 35.9	−03 15 10	B3	X
05 35 12.8	−00 44 07	B3	X
05 33 07.3	−01 43 02	B3	X
05 37 45.9	−00 46 42	B4	X
05 35 22.3	−04 25 28	B4	X
05 48 46.0	+00 43 32	B5	X
05 39 02.4	−05 11 40	B5	X
05 39 01.5	−02 38 56	B5	X
05 37 34.8	−01 25 20	B5	X
05 37 14.5	−01 40 04	B5	X
05 36 17.8	−01 38 07	B6	X
05 35 09.2	−00 16 11	B6	X
05 59 37.7	−01 26 39	B7	X
05 43 43.8	−00 56 19	B7	X
05 40 25.3	−04 25 16	B7	X
05 38 06.5	−00 11 03	B7	X
05 34 56.5	−00 07 22	B7	X
05 34 19.8	+04 49 30	B7	X
05 20 07.8	−05 50 46	B7	X
05 53 27.1	+00 46 45	B8	X
05 49 32.7	−00 40 55	B8	X
05 42 48.8	+04 51 09	B8	X
05 38 31.3	−00 08 52	B8	X
05 37 30.3	−00 14 25	B8	X
05 33 07.5	−05 20 26	B8	X
05 32 14.8	−04 31 06	B8	X
05 30 48.7	+00 01 43	B8	X
05 30 43.0	−05 29 27	B8	X
05 28 52.6	−00 36 11	B8	X
05 16 34.3	−05 03 41	B8	X
05 14 52.8	−04 37 36	B8	X
05 59 14.6	−04 21 34	B9	X
05 58 36.1	−02 05 57	B9	X
05 51 09.5	−04 34 57	B9	X
05 49 13.1	+01 27 30	B9	X
05 46 41.3	+02 14 27	B9	X
05 42 17.6	+02 22 02	B9	X
05 41 02.3	−02 43 01	B9	o
05 39 55.4	−03 19 50	B9	X
05 39 45.2	+04 26 05	B9	X
05 38 50.2	−04 16 18	B9	X
05 36 14.1	−02 15 32	B9	X
05 35 39.9	−03 18 58	B9	X
05 35 13.8	−02 22 52	B9	X
05 33 45.5	−00 01 44	B9	X
05 33 26.1	+00 37 17	B9	X
05 33 05.6	−01 43 16	B9	X
05 33 03.7	−01 14 28	B9	X
05 30 10.4	−05 12 06	B9	X
05 29 08.9	−05 47 28	B9	X
05 28 40.4	−02 44 01	B9	X
05 27 43.2	−00 15 33	B9	X
05 20 32.9	−05 17 17	B9	X
05 20 28.9	−05 48 44	B9	X
05 17 54.8	−04 29 24	B9	X
05 15 05.2	−05 15 09	B9	X
05 10 47.6	−05 10 11	B9	X
05 59 35.6	−04 20 15	A0	X
05 55 57.3	+00 50 10	A0	X
05 50 24.1	+01 46 43	A0	X
05 49 53.7	−00 11 01	A0	X
05 46 43.2	+02 42 26	A0	X

Table A11 – *continued*

RAJ2000 (h:m:s)	DEJ2000 (d:m:s)	SpT	K disk
05 46 12.4	−01 31 25	A0	X
05 44 48.6	−00 03 43	A0	X
05 43 11.9	−04 59 50	A0	o
05 42 58.8	−04 49 58	A0	X
05 40 40.6	−03 55 11	A0	X
05 35 37.5	−03 34 42	A0	X
05 32 49.8	−02 11 49	A0	X
05 56 26.6	−01 49 27	A1	X
05 34 23.7	+05 25 11	A1	X
05 31 21.2	−02 05 57	A1	X
05 50 28.6	−04 58 37	A2	X
05 50 23.9	+04 57 24	A2	X
05 38 09.2	−00 10 56	A2	o
05 16 06.6	−04 27 51	A2	X
05 45 15.1	−05 06 41	A3	X
05 26 16.3	−03 04 34	A3	X
05 52 22.6	−00 55 03	A4	X
05 37 40.5	−02 26 37	A4	X
05 32 16.7	−03 33 51	A4	X
05 56 49.4	−03 04 17	A5	X
05 50 13.1	+02 24 53	A5	X
05 44 18.8	+00 08 40	A9	o
05 26 41.1	−05 09 24	F0	X
05 31 18.4	−05 42 14	F1	X
05 02 44.0	−05 42 22	F1	X
05 44 16.9	−02 20 36	F2	X
05 57 01.0	−02 10 00	F4	X
05 31 04.7	−03 56 00	F5	X
05 18 26.7	−04 37 16	F6	X
05 40 24.4	+02 04 20	G3	X

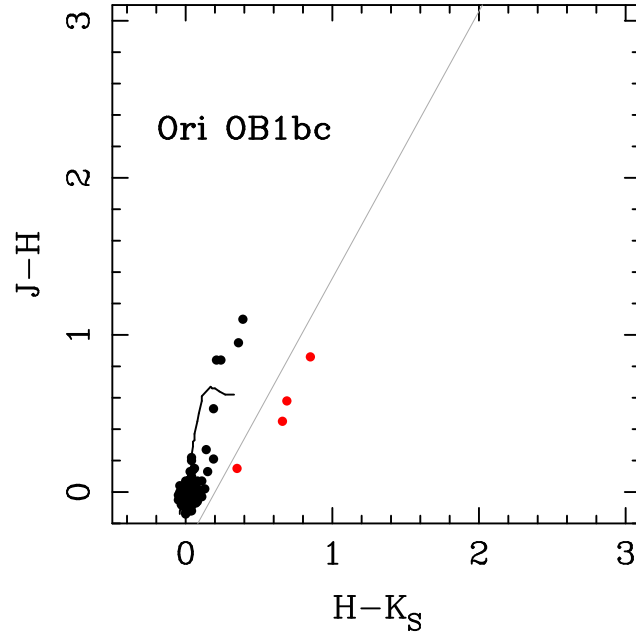


Figure A11. Ori OB1bc.

Table A12. Upper Sco.

Name	SpT	<i>K</i> disk	MIR disk
HIP 78168	B3V	X	X (−2.94)
HIP 78246	B5V	X	X (−2.93)
HIP 77858	B5V	X	X (−2.90)
HIP 79530	B6IV	X	X (−2.92)
HIP 77900	B7V	X	X (−2.94)
HIP 78207	B8Ia/Iab	X	o (−2.02)
HIP 80338	B8II	X	X (−2.86)
HIP 77909	B8III/IV	X	X (−2.92)
HIP 79739	B8V	X	X (−2.92)
HIP 78877	B8V	X	X (−2.90)
HIP 78956	B9.5V	X	X (−2.89)
HIP 78549	B9.5V	X	X (−2.93)
HIP 80024	B9II/III	X	X (−2.91)
HIP 80493	B9V	X	X (−2.91)
HIP 79897	B9V	X	X (−2.93)
HIP 79785	B9V	X	X (−2.89)
HIP 79771	B9V	X	X (−2.89)
HIP 79439	B9V	X	X (−2.83)
HIP 79410	B9V	X	X (−2.75)
HIP 78968	B9V	X	X (−3.01)
HIP 78809	B9V	X	X (−2.92)
HIP 78702	B9V	X	X (−2.90)
HIP 78530	B9V	X	X (−2.92)
HIP 77911	B9V	X	X (−2.88)
HIP 76633	B9V	X	X (−2.86)
HIP 76071	B9V	X	X (−2.94)
HIP 80311	A0V	X	X (−2.87)
HIP 79878	A0V	X	X (−2.88)
HIP 79860	A0V	X	X (−2.87)
HIP 79156	A0V	X	X (−2.77)
HIP 79124	A0V	X	X (−2.90)
HIP 78847	A0V	X	X (−2.88)
HIP 78196	A0V	X	X (−2.93)
HIP 78099	A0V	X	X (−2.92)
HIP 76310	A0V	X	X (−2.83)
HIP 80324	A0V+A0V	X	X (−2.88)
HIP 79733	A1mA9-F2	X	X (−2.88)
HIP 77545	A2/3V	X	X (−2.82)
HIP 79392	A2IV	X	X (−2.86)
HIP 78494	A2mA7-F2	X	X (−2.90)
HIP 79250	A3III/IV	X	X (−2.91)
HIP 82397	A3V	X	X (−2.90)
HIP 79366	A3V	X	X (−2.95)
HIP 77960	A4IV/V	X	X (−2.95)
HIP 77815	A5V	X	X (−2.88)
HIP 80059	A7III/IV	X	X (−2.77)
HIP 77457	A7IV	X	X (−2.91)
HIP 80130	A9V	X	X (−2.98)
HIP 80088	A9V	X	X (−2.77)
HIP 78996	A9V	X	X (−2.73)
HIP 78963	A9V	X	X (−2.96)
HIP 79643	F2	X	X (−2.84)
HIP 78233	F2/3IV/V	X	X (−2.84)
HIP 82319	F3V	X	X (−2.87)
HIP 80896	F3V	X	X (−2.93)
HIP 79097	F3V	X	X (−2.86)
HIP 79083	F3V	X	X (−2.89)
HIP 79644	F5	X	X (−2.85)
HIP 79606	F6	X	X (−2.84)
RX J1550.9-2534	F9	X	X (−2.83)

Table A12 – *continued*

[PZ99] J160000.7-250941	G0	X	X (−2.83)
HD 149598	G0	X	X (−2.79)
HD 146516	G0IV	X	X (−2.81)
HIP 78483	G0V	X	X (−2.80)
HD 147810	G1	X	X (−2.83)
[PZ99] J155812.7-232835	G2	X	X (−2.79)
HIP 79462	G2V	X	X (−2.80)
PPM 747978	G3	X	X (−2.81)
PPM 747651	G3	X	X (−2.78)
HD 142361	G3V	X	X (−2.78)
[PZ99] J161402.1-230101	G4	X	X (−2.75)
HD 142987	G4	X	X (−2.75)
[PZ99] J161459.2-275023	G5	X	X (−2.74)
PPM 732705	G6	X	X (−2.79)
RX J1541.1-2656	G7	X	X (−2.76)
[PZ99] J161618.0-233947	G7	X	X (−2.74)
SAO 183706	G8e	X	X (−2.81)
RX J1600.6-2159	G9	X	X (−2.78)
[PZ99] J161318.6-221248	G9	X	X (−2.75)
RX J1603.6-2245	G9	X	X (−2.77)
RX J1548.0-2908	G9	X	X (−2.78)
[PZ99] J161411.0-230536	K0	X	o (−1.18)
RX J1602.8-2401A	K0	X	X (−2.70)
[PZ99] J161933.9-222828	K0	X	X (−2.68)
[PZ99] J161329.3-231106	K1	X	X (−2.72)
ScoPMS 21	K1IV	X	X (−2.74)
[PZ99] J160814.7-190833	K2	X	X (−2.75)
[PZ99] J160421.7-213028	K2	X	X (−2.55)
ScoPMS 27	K2IV	X	X (−2.75)
[PZ99] J155847.8-175800	K3	X	X (−2.73)
[PZ99] J153557.8-232405	K3:	X	X (−2.75)
RX J1558.1-2405A	K4	X	X (−2.75)
[PZ99] J161302.7-225744	K4	X	X (−2.76)
[PZ99] J160251.2-240156	K4	X	X (−2.73)

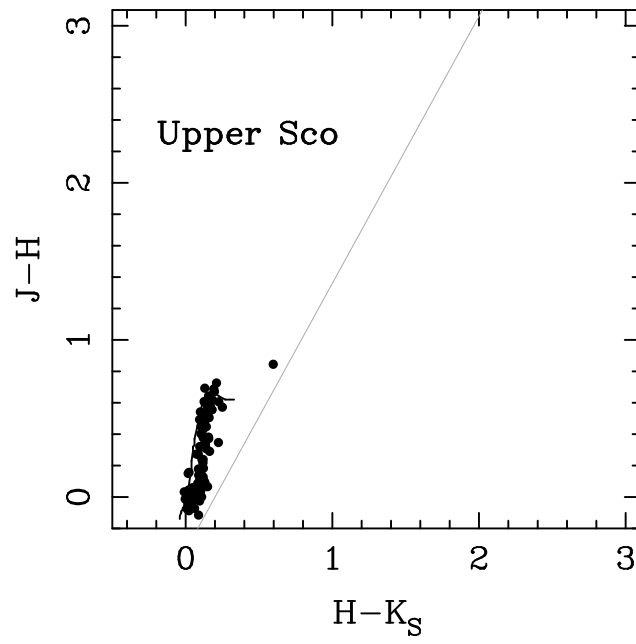


Figure A12. Upper Sco.

Table A13. NGC 2362.

RAJ2000 (h:m:s)	DEJ2000 (d:m:s)	SpT	<i>K</i> disk	MIR disk
07 18 58.40	-24 57 41.2	B3	X	X (-2.88)
07 18 36.85	-24 56 05.7	B3	X	X (-2.95)
07 18 40.81	-24 58 27.5	B5	X	X (-2.91)
07 18 45.74	-24 59 35.6	B7	X	X (-2.93)
07 18 38.10	-24 59 01.6	B9	X	X (-2.88)
07 18 54.54	-24 57 29.2	A0	X	X (-2.72)
07 18 35.48	-24 58 59.5	F2	X	X (-2.91)
07 18 34.01	-24 58 04.6	F2	X	X (-2.79)
07 18 48.54	-25 01 48.6	G2	X	X (-2.73)
07 18 46.89	-24 57 01.6	G6	X	X (-2.81)
07 18 59.61	-24 58 51.3	G8	X	X (-2.87)
07 18 32.46	-24 58 09.3	K1	X	X (-2.73)
07 18 24.51	-24 54 32.3	K1	X	X (-2.78)
07 18 43.36	-24 56 17.9	K2	X	X (-2.87)
07 18 40.20	-24 55 13.1	K2	X	X (-2.91)
07 18 46.46	-24 57 09.6	K3	X	X (-3.02)
07 18 31.63	-25 01 47.5	K3	X	X (-2.89)
07 18 50.90	-24 57 03.5	K4	X	X (-2.78)
07 18 35.31	-25 00 35.3	K4	X	X (-2.87)

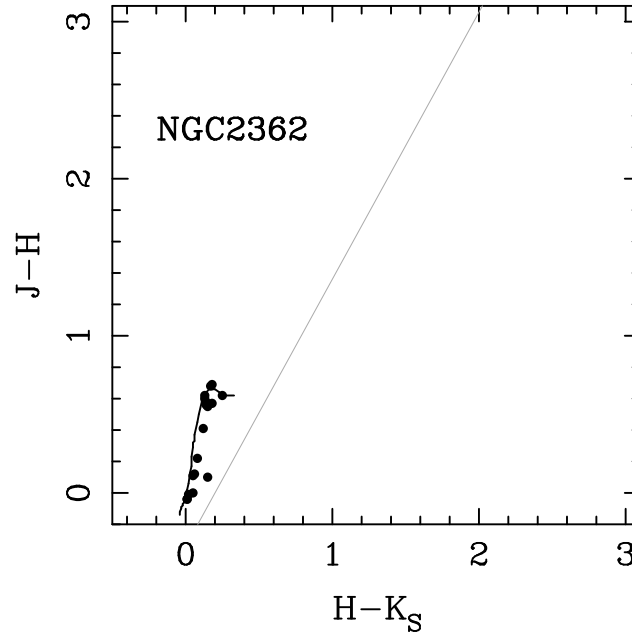
**Figure A13.** NGC 2362.

Table A14. γ Vel.

The spectral type with * mark is from SIMBAD database.

RAJ2000 (h:m:s)	DEJ2000 (d:m:s)	SpT	<i>K</i> disk	MIR disk
08 11 3929	−47 21 06.5	B2/B3III/IV	X	X (−2.89)
08 08 5123	−47 10 27.7	B3V	X	X (−2.87)
08 07 4074	−47 15 17.5	B8IV	X	X (−2.85)
08 08 2188	−47 09 28.6	B8Vne*	X	X (−2.72)
08 09 1107	−46 59 53.4	B9V	X	X (−2.80)
08 09 0430	−47 41 02.4	A0/A1V	X	X (−2.78)
08 08 2593	−47 36 06.9	A0V	X	X (−2.85)
08 09 0738	−47 38 13.6	A0V	X	X (−2.79)
08 11 1618	−47 13 18.8	A0V	X	X (−2.82)
08 09 1637	−47 13 37.4	A1/A2V	X	X (−2.80)
08 08 0690	−47 15 07.4	A1V	X	X (−2.85)
08 10 3253	−47 12 40.9	A2*	X	X (−2.86)
08 10 5813	−47 29 13.6	A2V	X	X (−2.85)
08 11 2187	−47 11 28.1	A5*	X	X (−2.82)
08 09 3482	−47 21 06.9	F0*	X	X (−2.86)
08 09 3763	−47 21 25.6	F0*	X	X (−2.78)
08 10 4836	−47 34 55.9	F5*	X	X (−2.79)

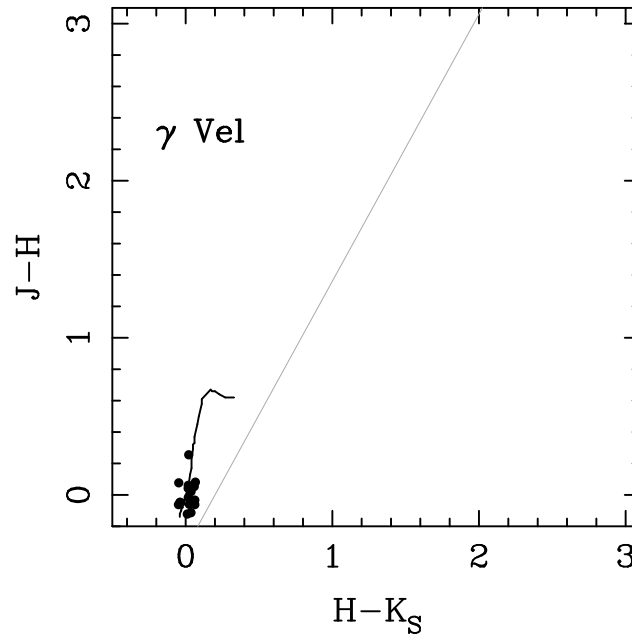


Figure A14. γ Vel.

Table A15. λ Ori.

Name	RAJ2000 (h:m:s)	DEJ2000 (d:m:s)	SpT	<i>K</i> disk	MIR disk
HD36895	05 35 1280	+09 36 47.8	B3	X	X (−2.91)
HD245203	05 35 1380	+09 41 49.4	B8	X	X (−2.89)
HD37035	05 35 5825	+09 31 54.1	B9	X	X (−2.84)
HD37110	05 36 2962	+09 37 54.2	B8	X	X (−2.75)
HD37051	05 36 0418	+09 49 55.0	B9	X	X (−2.77)
HD245140	05 34 5817	+09 56 26.7	B9	X	X (−2.81)
HD245168	05 35 02968	+09 56 04.1	B9	...	X (−2.78)
HD37034	05 35 5938	+09 42 48.0	A0	X	X (−2.73)
HD245185	05 35 0960	+10 01 51.5	A0	o	o (0.29)
HD245385	05 36 1338	+09 59 24.4	A0	...	X (−2.83)
HD244908	05 33 4712	+09 40 26.1	A2	...	X (−2.85)
HD245386	05 36 2132	+09 50 41.4	A2	...	X (−2.89)
HD37159	05 36 5811	+10 16 58.6	A3	X	X (−2.80)
...	05 34 4857	+09 30 57.1	A4	...	X (−2.73)
HD245275	05 35 4485	+09 55 24.3	A5	...	X (−2.83)
HD244927	05 33 5042	+10 04 21.1	A7	X	X (−2.87)
...	05 34 5914	+09 33 50.8	F3	...	X (−2.88)
299-3	05 36 0529	+10 21 27.1	F3	...	X (−2.87)
HD245370	05 36 0940	+10 01 25.4	F4	X	X (−2.58)
...	05 33 4028	+09 48 01.3	F6	...	X (−2.86)
...	05 33 5032	+09 58 18.5	F7	X	X (−2.86)
...	05 35 2468	+10 11 45.2	F7	...	X (−2.86)
HD244907	05 33 5115	+09 46 42.1	F8	X	X (−2.84)
h-star	05 35 0920	+10 02 51.8	F8	...	X (−2.87)
...	05 36 5226	+09 29 58.4	F9	...	X (−2.88)
...	05 35 4220	+10 13 44.7	G0	...	X (−2.83)

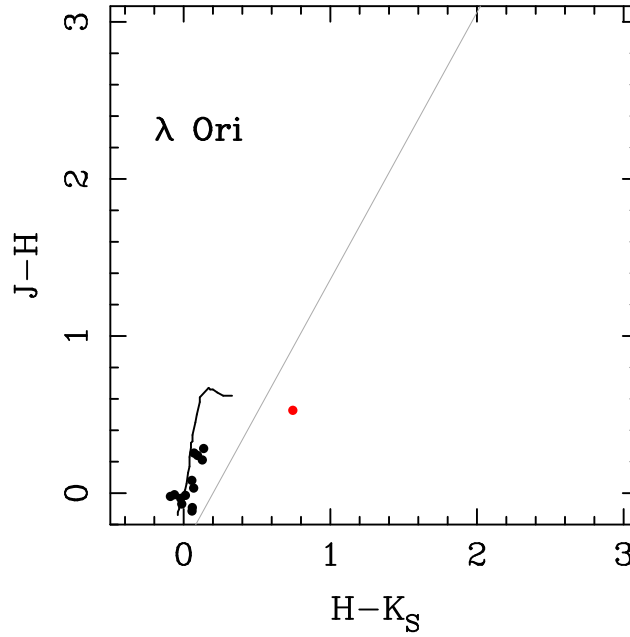
**Figure A15.** λ Ori.

Table A16. Per OB2.

RAJ2000 (h:m:s)	DEJ2000 (d:m:s)	SpT	K disk
04 06 39.0	+32 23 06	B3	X
03 47 52.7	+33 36 00	B3	X
03 47 25.7	+29 52 33	B3	X
04 06 55.8	+33 26 47	B4	X
03 49 07.3	+32 15 51	B6	X
03 25 50.1	+30 55 54	B6	X
03 50 51.3	+35 05 59	B7	X
03 44 40.7	+29 49 21	B7	X
03 55 58.7	+32 09 48	B8	X
04 12 45.2	+31 47 41	B9	X
04 07 24.5	+33 05 17	B9	X
04 02 56.6	+31 55 54	B9	X
03 58 35.5	+31 24 30	B9	X
03 55 54.9	+32 09 18	B9	X
03 54 20.7	+30 59 55	B9	X
03 44 51.3	+30 08 09	B9	X
03 28 17.4	+29 52 07	B9	X
03 20 53.5	+38 53 07	B9	X
03 07 51.0	+33 03 18	B9	X
03 06 35.1	+38 36 07	B9	X
03 58 55.5	+32 45 23	A0	X
03 34 57.9	+29 18 48	A0	X
03 11 57.6	+38 32 17	A0	X
03 10 06.3	+38 20 44	A0	X
03 03 11.3	+41 20 07	A1	X
03 40 40.3	+29 27 17	A5	X
03 02 23.6	+43 11 02	F8	X
03 36 00.0	+23 54 51	G4	X
03 55 06.9	+27 03 52	G5	X
03 22 11.9	+27 36 27	G6	X
03 46 09.5	+28 51 33	G8	X

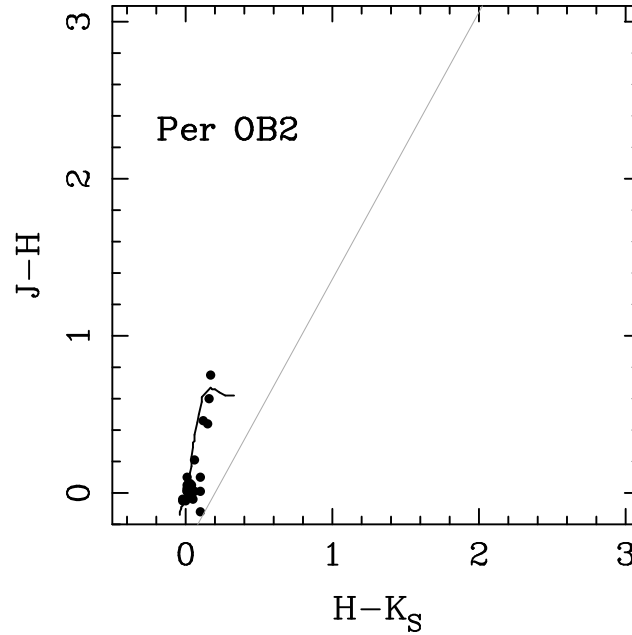


Figure A16. Per OB2.

Table A17. η Cha.

Name	RAJ2000 (h:m:s)	DEJ2000 (d:m:s)	SpT	K disk
η Cha	08 41 19.51	−78 57 48.1	B8V	X
HD 75505	08 41 44.71	−79 02 53.3	A1V	X
RS Cha	08 43 12.22	−79 04 12.3	A7V	X

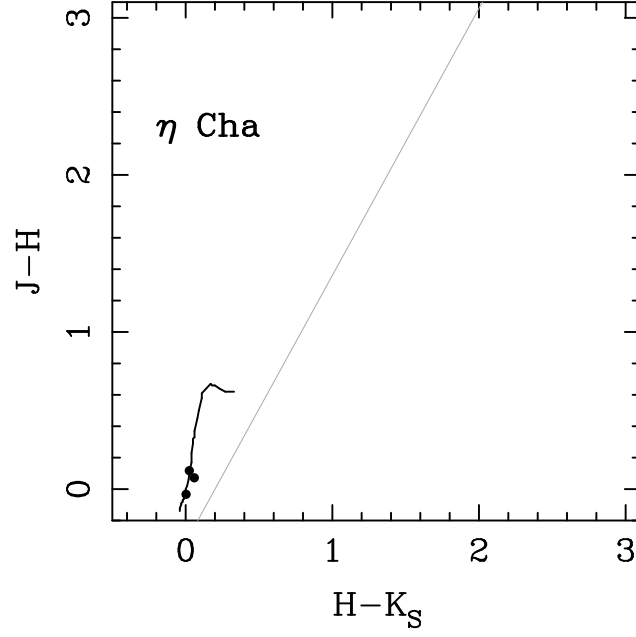
**Figure A17.** η Cha.

Table A18. Ori OB1a.

RAJ2000 (h:m:s)	DEJ2000 (d:m:s)	SpT	K disk
05 31 29.9	+01 41 24	B3	X
05 27 09.4	−01 22 02	B3	X
05 21 31.8	−00 24 59	B3	X
05 28 45.3	+01 38 38	B4	X
05 27 45.8	−02 08 44	B4	X
05 26 54.3	+03 36 53	B4	X
05 24 36.1	+02 21 11	B4	X
05 22 51.0	+03 33 08	B4	X
05 13 39.1	−03 37 19	B4	X
05 04 54.5	−03 02 23	B5	X
05 37 56.3	+00 59 15	B6	X
05 37 53.5	+00 58 07	B6	X
05 33 08.9	+03 07 52	B6	X
05 31 41.2	+02 49 58	B6	X
05 28 48.5	+02 09 53	B6	X
05 27 44.7	−01 48 47	B6	X
05 25 01.2	−02 48 56	B6	X
05 18 01.0	−00 02 16	B6	X
05 27 54.2	+01 06 18	B7	X
05 23 10.1	+01 08 23	B7	X
05 02 44.6	+03 27 28	B7	X
05 30 04.4	−01 44 59	B8	X
05 29 55.6	+02 08 32	B8	X
05 29 36.4	+05 13 38	B8	X
05 28 12.6	−01 56 29	B8	X
05 28 10.1	+00 47 14	B8	X
05 27 36.9	+01 06 27	B8	X
05 25 11.4	+01 55 24	B8	X
05 23 51.4	+00 51 46	B8	X
05 23 01.9	+01 41 49	B8	X
05 21 03.3	+04 28 41	B8	X
05 08 21.4	−02 17 23	B8	X
05 06 22.9	+02 40 24	B8	X
05 34 26.0	+01 21 37	B9	X
05 33 21.9	+02 22 36	B9	X
05 32 39.5	+02 05 32	B9	X
05 27 20.6	+02 12 57	B9	X
05 26 48.1	+02 04 06	B9	X
05 26 06.0	+00 50 02	B9	X
05 25 55.9	−02 20 08	B9	X
05 23 50.4	+02 04 56	B9	X
05 23 28.1	−01 00 09	B9	X
05 23 22.9	−01 26 27	B9	X
05 22 43.1	+00 08 21	B9	X
05 21 28.4	−01 32 46	B9	X
05 20 24.7	−03 30 35	B9	X
05 19 38.8	−01 06 31	B9	X
05 19 07.5	−01 05 56	B9	X
05 18 30.0	−01 08 18	B9	X
05 17 09.8	−02 34 48	B9	X
05 16 43.8	−00 53 20	B9	X
05 13 37.9	+04 12 40	B9	X
05 12 50.0	−01 33 49	B9	X
05 10 57.3	−01 45 50	B9	X
05 10 04.9	+02 56 09	B9	X
05 07 35.9	+04 32 30	B9	X
05 07 29.4	−03 18 41	B9	X
05 03 21.6	−02 58 57	B9	X
05 00 48.8	−00 30 03	B9	X
05 00 39.8	+03 15 55	B9	X
05 40 17.1	+00 58 21	A0	X
05 39 43.2	+00 54 27	A0	X
05 33 27.4	+02 39 06	A0	X

Table A18 – *continued*

RAJ2000 (h:m:s)	DEJ2000 (d:m:s)	SpT	<i>K</i> disk
05 27 15.8	+05 01 09	A0	X
05 22 57.8	−02 08 59	A0	X
05 19 40.1	−01 21 22	A0	X
05 19 03.5	+00 26 19	A0	X
05 05 54.6	+01 51 08	A0	X
05 05 04.2	−01 18 41	A0	X
05 28 10.5	−01 46 18	A1	X
05 22 38.8	−01 02 34	A1	X
05 14 37.0	+02 33 49	A1	X
05 05 01.0	+02 38 44	A1	X
05 03 21.7	−00 00 16	A1	X
05 30 52.6	+01 36 41	A2	X
05 18 29.9	+02 05 29	A2	X
05 13 26.8	−02 37 37	A2	X
05 24 08.0	+02 27 47	A3	o
05 23 53.3	−03 04 59	A3	X
05 15 57.6	+01 19 39	A3	X
05 08 06.4	+03 44 55	A3	X
05 20 52.9	+01 01 00	A4	X
05 18 24.3	−02 32 07	A5	X
05 36 29.4	+03 18 30	A6	X
05 28 09.6	+03 37 23	A6	X
05 02 43.5	+05 49 50	A7	X
05 30 53.3	+05 41 34	A8	X
05 24 42.8	+01 43 48	A8	o
05 15 46.4	−01 16 40	A8	X
05 28 10.7	+02 22 35	F1	X
05 02 19.0	−01 11 55	F1	X
05 00 34.4	+00 00 20	F1	X
05 37 48.2	+02 44 47	F3	X
05 36 41.8	+02 41 11	F4	X
05 19 36.8	+01 33 02	F7	X
05 08 12.6	+01 08 36	G1	X
05 05 38.6	+01 27 31	G1	X
05 02 15.1	−01 43 08	G6	X

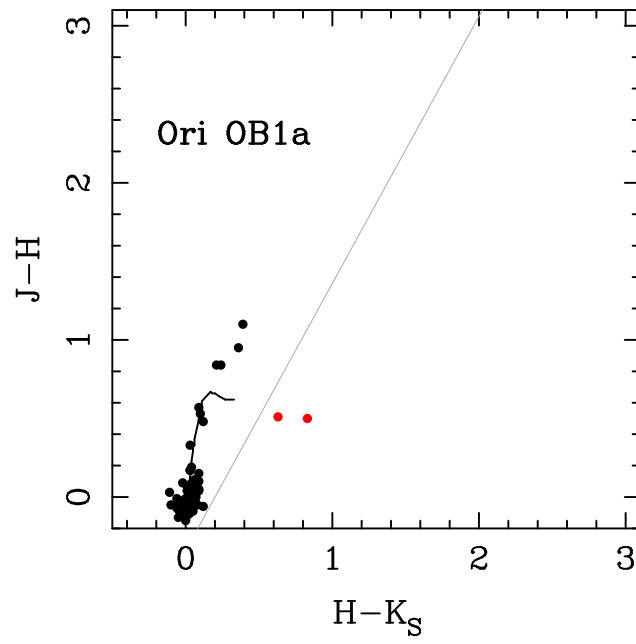


Figure A18. Ori OB1a.

Table A19. NGC 7160.

Name	RAJ2000 (h:m:s)	DEJ2000 (d:m:s)	SpT	<i>K</i> disk	MIR disk
DG-513	21 52 32.89	+62 23 56.9	B5.0	X	X (−2.42)
DG-32	21 54 22.86	+62 27 55.3	B5.5	X	X (−2.80)
DG-940	21 56 07.66	+62 34 06.9	B8.5	X	X (−2.52)
DG-37	21 54 19.40	+62 28 06.7	B9.0	X	X (−2.91)
DG-424	21 51 55.66	+62 27 13.8	B9.0	X	X (−2.96)
DG-36	21 54 14.24	+62 45 57.7	B9.5	X	X (−2.99)
DG-720	21 54 02.85	+62 26 34.8	A0.0	X	X (−2.86)
DG-39	21 53 27.80	+62 35 18.7	A0.0	X	X (−2.68)
DG-460	21 52 11.46	+62 38 45.6	A0.0	X	X (−2.96)
DG-682	21 53 45.12	+62 36 54.8	A2.0	X	X (−2.57)
DG-529	21 52 39.25	+62 44 49.5	A2.0	X	X (−2.91)
DG-934	21 56 03.59	+62 38 54.8	A2.5	X	X (−2.95)
DG-853	21 55 07.13	+62 43 33.7	A2.5	X	X (−2.65)
DG-45	21 53 45.51	+62 40 57.4	A3.0	X	X (−2.98)
DG-67	21 52 59.85	+62 42 06.4	A4.0	X	X (−2.76)
DG-920	21 55 54.91	+62 44 33.4	A4.5	X	X (−2.87)
DG-954	21 56 15.84	+62 45 44.1	A5.0	X	...
DG-47	21 53 55.61	+62 36 18.0	A5.0	X	X (−2.82)
DG-687	21 53 46.15	+62 46 35.4	A5.0	X	X (−2.90)
DG-946	21 56 10.81	+62 34 54.9	A5.5	X	X (−2.43)
DG-409	21 51 45.66	+62 42 58.2	A5.5	X	X (−2.99)
DG-42	21 53 36.84	+62 32 48.5	A6.0	X	X (−2.99)
DG-398	21 51 42.28	+62 33 14.5	A6.0	X	X (−2.92)
DG-685	21 53 45.42	+62 45 25.0	A6.5	X	X (−3.04)
DG-382	21 51 31.43	+62 28 46.2	A6.5	X	X (−2.86)
DG-907	21 55 43.05	+62 42 28.9	A7.0	X	X (−2.93)
DG-65	21 54 36.79	+62 33 59.5	A7.0	X	X (−2.87)
DG-526	21 52 38.57	+62 45 52.3	A7.0	X	X (−2.96)
DG-481	21 52 21.13	+62 45 03.4	A7.0	X	o (−1.75)
DG-794	21 54 33.51	+62 47 53.1	A8.0	X	X (−2.83)
DG-49	21 53 51.91	+62 33 24.5	A8.0	X	X (−2.92)
DG-531	21 52 39.31	+62 46 58.1	A8.0	X	X (−2.50)
DG-725	21 54 05.40	+62 43 42.7	A8.5	X	X (−2.95)
DG-899	21 55 38.35	+62 45 53.0	A9.0	X	X (−2.85)
DG-399	21 51 41.82	+62 47 13.8	F0.0	X	X (−2.90)
DG-408	21 51 45.44	+62 47 05.3	F0.5	X	X (−2.95)
DG-48	21 54 13.27	+62 43 09.2	F1.0	X	X (−2.86)
DG-952	21 56 14.29	+62 41 41.7	F1.5	X	X (−2.93)
DG-60	21 54 33.59	+62 28 52.9	F1.5	X	X (−2.89)
DG-41	21 53 19.42	+62 37 38.7	F2.0	X	X (−2.90)
DG-936	21 56 05.45	+62 26 53.5	F2.5	X	X (−2.86)
DG-52	21 55 19.88	+62 39 15.0	F3.0	X	X (−2.93)
DG-55	21 53 33.08	+62 37 03.1	F3.0	X	X (−2.94)
DG-58	21 54 15.89	+62 36 04.5	F3.5	X	X (−2.94)
DG-472	21 52 20.24	+62 27 58.8	F4.5	X	X (−2.71)
DG-423	21 51 54.64	+62 44 06.7	F4.5	X	X (−2.83)
DG-949	21 56 11.16	+62 47 04.6	F5.0	X	...
DG-59	21 54 39.40	+62 36 21.9	F5.0	X	X (−2.97)
DG-62	21 54 30.34	+62 31 15.7	F5.0	X	X (−2.62)
DG-603	21 53 07.41	+62 27 19.6	F5.0	X	X (−2.87)
DG-394	21 51 38.59	+62 35 50.6	F5.0	X	X (−2.98)
DG-392	21 51 37.31	+62 38 06.5	F5.0	X	X (−2.82)
DG-912	21 55 47.60	+62 35 43.2	F5.5	X	o (−2.19)
DG-533	21 52 40.42	+62 46 06.6	F5.5	X	X (−2.93)
DG-825	21 54 52.61	+62 45 28.2	F6.0	X	X (−2.87)
DG-921	21 55 55.07	+62 43 55.5	F6.5	X	X (−2.88)
DG-422	21 51 54.87	+62 38 34.6	F6.5	X	X (−2.84)
DG-64	21 53 22.52	+62 34 24.9	F7.0	X	X (−2.77)
DG-40	21 52 49.71	+62 31 30.9	F7.0	X	X (−2.91)
DG-61	21 53 30.14	+62 30 09.7	F8.0	X	X (−2.96)
DG-414	21 51 46.81	+62 46 11.6	F8.0	X	X (−2.91)
DG-644	21 53 27.03	+62 44 50.4	F8.5	X	X (−2.97)

Table A19 – *continued*

Name	RAJ2000 (h:m:s)	DEJ2000 (d:m:s)	SpT	<i>K</i> disk	MIR disk
DG-462	21 52 12.89	+62 44 08.6	F8.5	X	X (−2.84)
DG-50	21 53 35.48	+62 30 03.2	F9.0	X	X (−2.88)
DG-349	21 51 17.53	+62 43 41.1	F9.5	X	X (−2.94)
DG-56	21 54 07.28	+62 44 26.0	G0.5	X	X (−2.92)
DG-455	21 52 09.98	+62 25 31.2	G2.0	X	X (−2.96)
DG-895	21 55 36.36	+62 43 53.8	G2.5	X	X (−2.86)
DG-371	21 51 26.25	+62 29 16.1	G3.5	X	X (−2.88)
[SHB2004] 03-180	21 53 54.11	+62 38 10.2	F9	X	X (−2.78)
[SHB2004] 03-479	21 54 17.22	+62 41 33.8	G0	X	X (−2.88)
[SHB2004] 03-872	21 53 52.96	+62 45 24.8	G0	X	...
[SHB2004] 03-791	21 54 56.24	+62 44 42.2	G2	X	X (−2.68)
[SHB2004] 03-228	21 53 59.59	+62 38 43.3	G2	X	X (−2.88)
[SHB2004] 03-654	21 53 58.11	+62 43 21.3	G2	X	X (−2.89)
[SHB2004] 04-1027	21 53 07.62	+62 46 14.4	G2	X	X (−2.93)
[SHB2004] 01-615	21 52 35.60	+62 29 08.2	G2	X	X (−2.77)
[SHB2004] 03-835	21 54 04.98	+62 45 04.8	G3.5	X	X (−2.91)
[SHB2004] 02-592	21 54 08.60	+62 30 14.0	G4	X	...
[SHB2004] 04-521	21 52 58.91	+62 41 34.7	G4	X	X (−2.84)
[SHB2004] 03-500	21 55 04.86	+62 41 47.9	G5	X	X (−2.84)
[SHB2004] 01-1164	21 53 32.07	+62 34 05.3	G5.5	X	X (−2.91)

This paper has been typeset from a \TeX / \LaTeX file prepared
by the author.

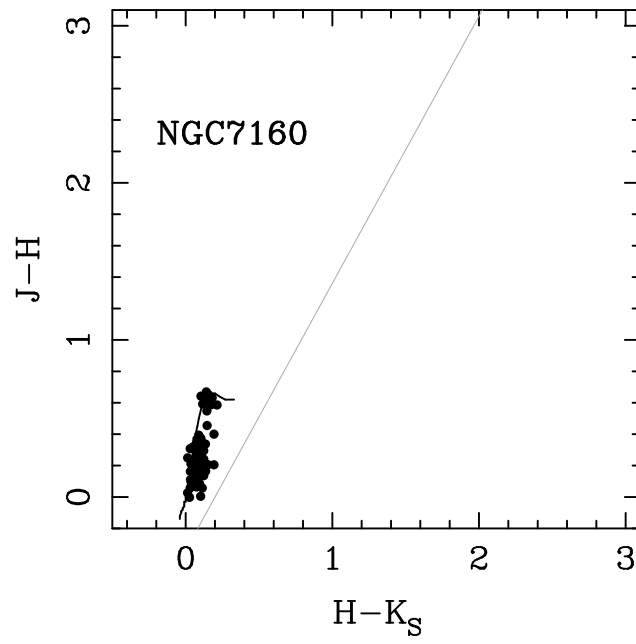


Figure A19. NGC 7160.